The impact of the South-East Madagascar Bloom on the oceanic CO2 sink

Nicolas Metzl, Claire Lo Monaco, Coraline Leseurre, Céline Ridame, Jonathan Fin, Claude Mignon, Marion Gehlen, Thi Tuyet Trang Chau

Biogeosciences, 19, 1451–1468, 2022
https://doi.org/10.5194/bg-19-1451-2022

Biogeosciences
Open Access
EGU

The impact of the South-East Madagascar Bloom on the oceanic CO_2 sink

Nicolas Metzl[1], Claire Lo Monaco[1], Coraline Leseurre[1], Céline Ridame[1], Jonathan Fin[1], Claude Mignon[1], Marion Gehlen[2], and Thi Tuyet Trang Chau[2]

[1]Laboratoire LOCEAN (IPSL), Sorbonne Université, CNRS–IRD–MNHN, Paris, 75005, France
[2]Laboratoire LSCE (IPSL), Université Paris-Saclay, CEA–CNRS–UVSQ, Gif-sur-Yvette, 91191, France

Correspondence: Nicolas Metzl (nicolas.metzl@locean.ipsl.fr)

Received: 22 October 2021 – Discussion started: 3 November 2021
Revised: 29 January 2022 – Accepted: 8 February 2022 – Published: 10 March 2022

Abstract. We described new sea surface CO_2 observations in the south-western Indian Ocean obtained in January 2020 when a strong bloom event occurred south-east of Madagascar and extended eastward in the oligotrophic Indian Ocean subtropical domain. Compared to previous years (1991–2019) we observed very low fCO_2 and dissolved inorganic carbon concentrations (C_T) in austral summer 2020, indicative of a biologically driven process. In the bloom, the anomaly of fCO_2 and C_T reached respectively -33 µatm and -42 µmol kg^{-1}, whereas no change is observed for alkalinity (A_T). In January 2020 we estimated a local maximum of air–sea CO_2 flux at 27° S of -6.9 mmol m^{-2} d^{-1} (ocean sink) and -4.3 mmol m^{-2} d^{-1} when averaging the flux in the band 26–30° S. In the domain 25–30° S, 50–60° E we estimated that the bloom led to a regional carbon uptake of about -1 TgC per month in January 2020, whereas this region was previously recognized as an ocean CO_2 source or near equilibrium during this season. Using a neural network approach that reconstructs the monthly fCO_2 fields, we estimated that when the bloom was at peak in December 2019 the CO_2 sink reached -3.1 (± 1.0) mmol m^{-2} d^{-1} in the band 25–30° S; i.e. the model captured the impact of the bloom. Integrated in the domain restricted to 25–30° S, 50–60° E, the region was a CO_2 sink in December 2019 of -0.8 TgC per month compared to a CO_2 source of $+0.12$ (± 0.10) TgC per month in December when averaged over the period 1996–2018. Consequently in 2019 this region was a stronger CO_2 annual sink of -8.8 TgC yr^{-1} compared to -7.0 (± 0.5) TgC yr^{-1} averaged over 1996–2018. In austral summer 2019–2020, the bloom was likely controlled by a relatively deep mixed-layer depth during the preceding winter (July–September 2019) that would supply macro- and/or micro-nutrients such as iron to the surface layer to promote the bloom that started in November 2019 in two large rings in the Madagascar Basin. Based on measurements in January 2020, we observed relatively high N_2 fixation rates (up to 18 nmol N L^{-1} d^{-1}), suggesting that diazotrophs could play a role in the bloom in the nutrient-depleted waters. The bloom event in austral summer 2020, along with the new carbonate system observations, represents a benchmark case for complex biogeochemical model sensitivity studies (including the N_2 fixation process and iron supplies) for a better understanding of the origin and termination of this still "mysterious" sporadic bloom and its impact on ocean carbon uptake in the future.

1 Introduction

In the south-western subtropical Indian Ocean a phytoplankton bloom, called the South-East Madagascar Bloom (SEMB), occurs sporadically during austral summer (December–March, Fig. 1). Based on the first years of SeaWiFS (Sea-Viewing Wide Field-of-View Sensor) satellite chlorophyll *a* (Chl *a*) observations in 1997–2001, the SEMB was first recognized by Longhurst (2001) as the largest bloom in the subtropics, extending over 3000 km × 1500 km in the Madagascar Basin. When the SEMB is well developed like in February–March 1999 (Longhurst, 2001), monthly mean Chl *a* concentrations are higher than 0.5 mg m^{-3} within the bloom, contrasting with the low Chl *a* in the surrounding oligotrophic waters (<0.05 mg m^{-3}). For reasons still not fully understood, this bloom occurred in specific

years (1997, 1999 and 2000) but was absent or moderate during a strong El Niño–Southern Oscillation (ENSO) event in 1998. Following the first study by Longhurst (2001), the frequency, extension, levels of Chl *a* concentration, and processes that would control the SEMB and its variability have been investigated in several studies (Srokosz et al., 2004; Uz, 2007; Wilson and Qiu, 2008; Poulton et al., 2009; Raj et al., 2010; Huhn et al., 2012; Srokosz and Quartly, 2013). Most of these studies were based on Chl *a* derived from remote sensing and altimetry. They all concluded the need for in situ observations to understand the initiation, extent and termination of the SEMB. To our knowledge in situ biogeochemical observations (Chl *a*, phytoplanktonic species and nutrients) within the SEMB region were only obtained during MadEx (Madagascar Experiment) in February 2005 (Poulton et al., 2009; Srokosz and Quartly, 2013), a year when the bloom was not well developed (e.g. Uz, 2007; Wilson and Qiu, 2008). The MadEx cruise was conducted above the Madagascar Ridge and west of 51° E in the Madagascar Basin. However, the eastward extension of the SEMB occasionally reached the central oligotrophic Indian Ocean subtropics (longitude of 70° E, Fig. 1b) where the bloom is transported and apparently bounded by the South Indian Counter Current (SICC) around 25° S (Siedler et al., 2006; Palastanga et al., 2007; Huhn et al., 2012; Menezes et al., 2014). A recent analysis of the East Madagascar Current (EMC) and its retroflection near the southern tip of Madagascar also suggests that a complex dynamic sometimes promotes the SEMB (Ramanantsoa et al., 2021). Modelling studies also suggested an eastward propagation of the SEMB through advection or eddy transport originating from the south-eastern coast of Madagascar (Lévy et al., 2007; Srokosz et al., 2015; Dilmahamod et al., 2020), but a precise explanation of the internal (e.g. local upwelling, Ekman pumping and mesoscale dynamics) or external processes (e.g. iron from rivers, coastal zones or sediments) at the origin of this "mysterious" bloom is still missing.

The above studies have been recently synthesized by Dilmahamod et al. (2019), who also proposed an index to determine the level of the SEMB (strong, moderate or absent) based on the difference in Chl *a* concentrations between the western and eastern regions centred respectively around 55 and 80° E at 24–28° S. Quoting Dilmahamod et al. (2019), "The South-East Madagascar Bloom is one of the largest blooms in the world. It can play a major role in the fishing industry, as well as capturing carbon dioxide from the atmosphere." Although numerous cruises measuring sea surface CO_2 fugacity (fCO_2) have been conducted since the 1990s in the south-western Indian Ocean region (Poisson et al., 1993; Metzl et al., 1995; Sabine et al., 2000; Metzl, 2009), the impact of the SEMB on air–sea CO_2 fluxes was not previously investigated. This is probably because the bloom was not strong enough at the time of the cruises to identify large fCO_2 anomalies in this region. Therefore, the temporal (seasonal and/or inter-annual) fCO_2 variability in the western and subtropical Indian Ocean is generally interpreted by thermodynamics as the main control, with biological activity and mixing processes being secondary driving processes in this oligotrophic region (Louanchi et al., 1996; Metzl et al., 1998; Sabine et al., 2000; Takahashi et al., 2002). On the other hand, all climatologies based on observations suggest rather homogeneous sea surface fCO_2 or dissolved inorganic carbon (C_T) fields in this region (Takahashi et al., 2002, 2009, 2014; Lee et al., 2000; Sabine et al., 2000; Bates et al., 2006; Lauvset et al., 2016; Zeng et al., 2017; Broullón et al., 2020; Keppler et al., 2020; Fay et al., 2021; Gregor and Gruber, 2021). This suggests that, although the SEMB and its extent have been regularly observed since 1997, it seems to have a small effect on fCO_2 or C_T spatial variations. However, in austral summer 2019/20, the SEMB was particularly pronounced, reaching monthly mean Chl *a* concentrations up to 2.5 mg m^{-3} at the peak of the bloom in December 2019. It was clearly much stronger than previously observed, at least since 1997 (Fig. 1), and reflected in fCO_2 observations in this region (Fig. 2).

In this analysis, we describe new oceanic carbonate system observations in surface waters obtained in January 2020 associated with this very strong SEMB event and compare these observations with climatological values and previous fCO_2 data when the SEMB was not well developed. We also evaluate the impact of the bloom on air–sea CO_2 fluxes based on both observations and reconstructed monthly fCO_2 fields in the south-western Indian Ocean.

2 Data collection

As part of the long-term OISO project (Océan Indien Service d'Observations), the OISO-30 cruise was conducted in austral summer 2020 (from 2 January to 6 February 2020) onboard the RV *Marion Dufresne* in the southern Indian Ocean (part of the track shown in Fig. 1). During the cruise, underway continuous surface measurements were obtained for temperature (SST), salinity (SSS), the fugacity of CO_2 (fCO_2), the total alkalinity (A_T) and the total dissolved inorganic carbon (C_T). Analytical methods followed the protocol used since 1998 and previously described for other OISO cruises (e.g. Metzl et al., 2006; Metzl, 2009; Lo Monaco et al., 2021). Sea surface temperature and salinity were measured continuously using an SBE45 thermosalinograph. Salinity data were controlled by regular sampling and conductivity measurements (Guildline Autosal 8400B and using the IAPSO – International Association for the Physical Sciences of the Oceans – standard or OSIL – Ocean Scientific International). The SST and SSS data were also checked against CTD (conductivity–temperature–depth) surface records when available. Accuracies of SST and SSS are respectively 0.005 °C and 0.01. Total alkalinity (A_T) and total dissolved inorganic carbon (C_T) were measured continuously in surface water (three to four samples per

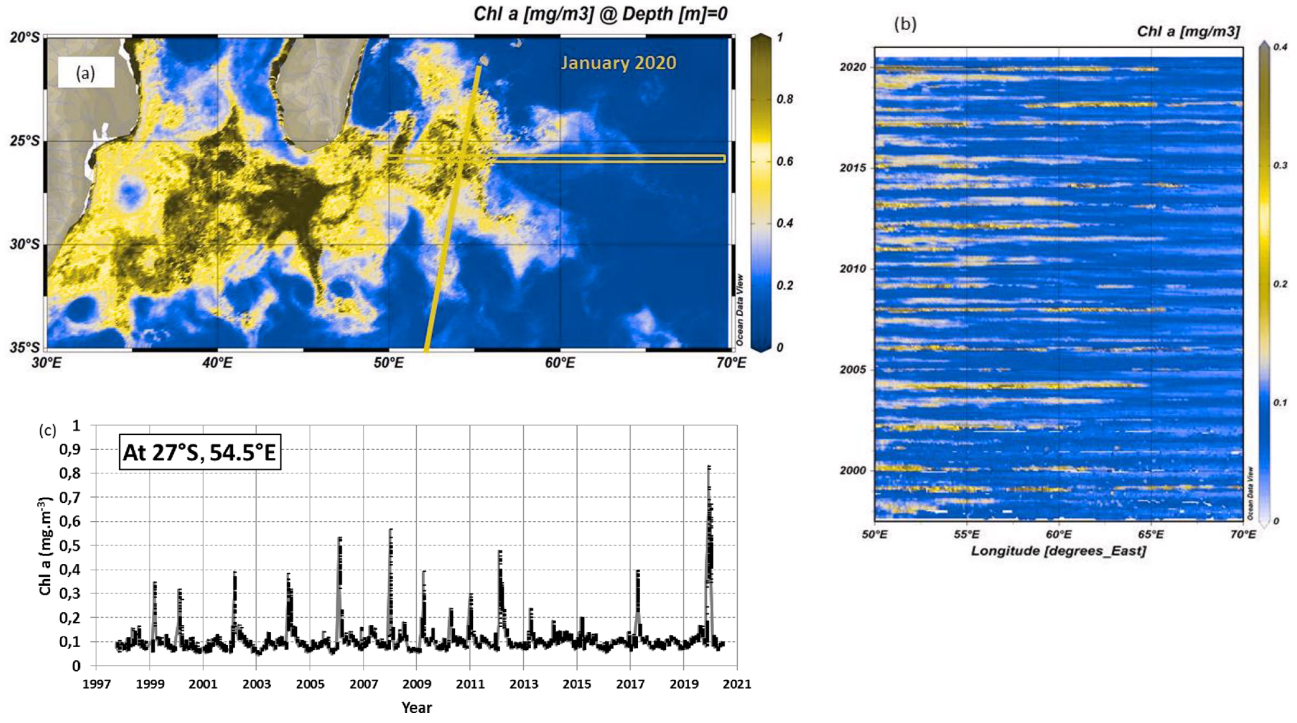

Figure 1. **(a)** Map of monthly surface Chl *a* ($mg\,m^{-3}$) in the south-western Indian Ocean in January 2020 derived from MODIS data (4 km × 4 km resolution), highlighting the bloom south and south-east of Madagascar. **(b)** Hovmoller time series (time and longitude) of Chl *a* ($mg\,m^{-3}$) around 26.5° S along 50–70° E (orange box in **a**). **(c)** Time series of monthly Chl *a* ($mg\,m^{-3}$) at 27° S, 54.5° E (only when the valid number of pixels is greater than five for each point). The orange line on the map identifies the track of the OISO-30 cruise. The figures highlight the high Chl *a* concentration in austral summer 2020. Panels **(a)** and **(b)** produced with ODV (Ocean Data View; Schlitzer, 2013) from data downloaded from https://resources.marine.copernicus.eu/ (OCEANCOLOUR_GLO_CHL_L4_REP_OBSERVATIONS_009_093, last access: 10 April 2021).

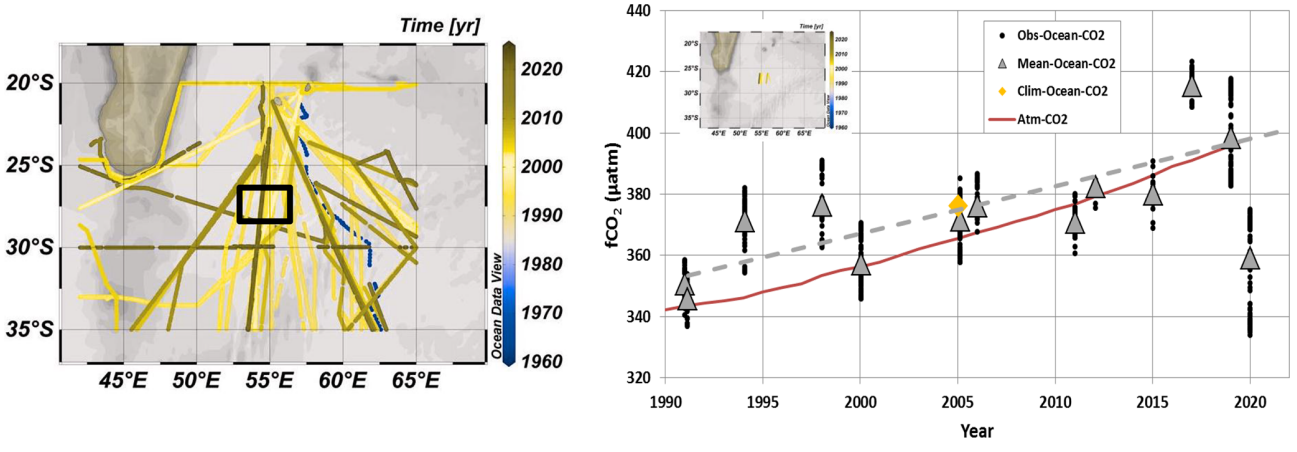

Figure 2. On the left are shown tracks of cruises with sea surface fCO_2 data available in the south-western Indian Ocean in the SOCAT data product (Surface Ocean CO_2 Atlas; SOCAT v2021, Bakker et al., 2016, 2021). On the right is shown a time series of fCO_2 data (black dots) and mean fCO_2 for each period (grey triangles) at 27–28° S, 55° E (black square in the map and insert on the right) for the months of January and February (data available from 1991 to 2020 for austral summer). The red curve is the atmospheric fCO_2. Although over 1991–2019 the ocean fCO_2 increased by $+1.55$ (± 0.40) $\mu atm\,yr^{-1}$ (dashed grey line) due to anthropogenic CO_2 uptake, the fCO_2 recorded in January 2020 in the bloom were low compared to previous years with some values below 340 µatm, i.e. lower than in 1991. The January–February-averaged fCO_2 in the same region derived from the 2005 climatology of Takahashi et al. (2014) is also plotted (orange diamond). Map on the left produced with ODV (Schlitzer, 2013).

hour) using a potentiometric titration method (Edmond, 1970) in a closed cell. For calibration, we used the certified reference materials (CRMs, batch no. 173) provided by Andrew Dickson (SIO – Scripps Institution of Oceanography, University of California). Replicate measurements were occasionally performed at the same location. At 30° S, 54° E for four replicates the mean A_T and C_T concentrations were respectively 2328.6 (±0.7) and 1998.2 (±1.6) µmol kg^{-1}. At 35° S, 53.5° E for six replicates the mean A_T and C_T were 2340.5 (±0.6) and 2060.6 (±1.1) µmol kg^{-1}. Overall, we estimated the accuracy for both A_T and C_T to be better than 3 µmol kg^{-1} (based on the analysis of CRMs). Like for all other OISO cruises, the surface underway A_T and C_T data will be available on the National Centers for Environmental Information (NCEI) Ocean Carbon and Acidification Data System (OCADS) (https://www.ncei.noaa.gov/access/ocean-carbon-data-system/oceans/VOS_Program/OISO.html, last access: 3 March 2022).

For fCO_2 measurements, sea surface water was continuously equilibrated with a "thin-film" type equilibrator thermostated with surface seawater (Poisson et al., 1993). The xCO_2 in the dried gas was measured with a non-dispersive infrared analyser (NDIR, Siemens Ultramat 6F). Standard gases for calibration (271.39, 350.75 and 489.94 ppm) were measured every 6 h. To correct xCO_2 dry measurements to fCO_2 in situ data, we used polynomials given by Weiss and Price (1980) for vapour pressure and by Copin-Montégut (1988, 1989) for temperature (temperature in the equilibrium cell measured using SBE38 was on average 0.28 °C warmer than SST during the OISO-30 cruise). The oceanic fCO_2 data for this cruise are available in the SOCAT (Surface Ocean CO_2 Atlas) data product (v2021, Bakker et al., 2016, 2021) and at NCEI OCADS (Lo Monaco and Metzl, 2021). Note that when added to SOCAT, the original fCO_2 data are recomputed (Pfeil et al., 2013) using temperature correction from Takahashi et al. (1993). Given the small difference between SST and equilibrium temperature, the fCO_2 data from our cruises are identical (within 1 µatm) in SOCAT and NCEI OCADS. For coherence with other cruises we used the fCO_2 values as provided by SOCAT.

During the OISO-30 cruise, silicate (Si) concentrations in surface and water column samples (filtered at 0.2 µm, poisoned with 100 µL $HgCl_2$ and stored at 5° C) were measured onshore by colorimetry (Aminot and Kérouel, 2007; Coverly et al., 2009). Based on replicate measurements for deep samples collected during OISO cruises we estimate an error of about 0.3 % in Si concentrations.

Unfiltered and 20 µm prefiltered seawater (∼ 10 m depth) were collected for the determination of net N_2 fixation in both the total fraction and the size fraction lower than 20 µm using the $^{15}N_2$ gas tracer addition method (Montoya et al., 1996). As a difference, we calculated N_2 fixation rates related to the microphytoplankton size class (>20 µm). Immediately after sampling, 2.5 mL of 99 % $^{15}N_2$ (Eurisotop) was introduced to 2.3 L polycarbonate bottles through a butyl septum. $^{15}N_2$ tracer was added to obtain a ∼ 10 % final enrichment. Then, each bottle was vigorously shaken and incubated in an on-deck incubator with circulating seawater and equipped with a blue filter to simulate the level of irradiance at the sampling depth. After 24 h incubation, 2.3 L was filtered onto pre-combusted 25 mm GF/F filters, and filters were stored at −25° C. Sample filters were dried at 40 °C for 48 h before analysis. Nitrogen (N) content of particulate matter and its ^{15}N isotopic ratio were quantified using an online continuous flow elemental analyser (Flash 2000 HT), coupled with an isotopic ratio mass spectrometer (DELTA V Advantage via a ConFlow IV interface from Thermo Fisher Scientific). N_2 fixation rates were calculated by isotope mass balanced as described by Montoya et al. (1996). The detection limit for N_2 fixation, calculated from significant enrichment and the lowest particulate nitrogen is estimated to 0.04 nmol N L^{-1} d^{-1}.

Other data used in this analysis (e.g. Chl *a* from remote sensing; ADCP, acoustic Doppler current profiler; current fields; fCO_2; A_T; and C_T from other cruises or from climatology) will be referred to in the next sections when appropriate.

3 Reconstructed fCO_2 and air–sea CO_2 fluxes

In order to complement the results based on regional in situ data and evaluate the CO_2 sink anomalies in this region back to 1996, we also used results from a neural network model that reconstructs monthly fCO_2 fields and air–sea CO_2 fluxes. The fCO_2 fields were obtained from an ensemble-based feed-forward neural network model (named CMEMS-LSCE-FFNN, Copernicus Marine Environment Monitoring Service–Laboratoire des Sciences du Climat et de l'Environnement feed-forward neural network) described in Chau et al. (2022). This ensemble-based approach is an updated and improved version of the model by Denvil-Sommer et al. (2019). Model results are annually qualified and distributed by the Copernicus Marine Environment Monitoring Service (CMEMS, Chau et al., 2020). To take into account the period in austral summer 2020 when the SEMB was particularly strong, we used the latest temporal extension of the model which relies on the most recent version of the SOCAT database (SOCAT v2021, Bakker et al., 2021). For a full description of the model, access to the data and a statistical evaluation of fCO_2 reconstructions, please refer to Chau et al. (2022).

4 Results

4.1 Sea surface fCO_2, C_T and A_T distributions in the SEMB in January 2020

In January 2020, the SEMB occupied a large region in the southern section of the Mozambique Channel, the Natal Basin, the Mozambique Plateau and the Madagascar Basin. It extended eastward with mesoscale and filaments structures reaching 60° E in the southern subtropical Indian Ocean, where Chl *a* was up to 0.5 mg m^{-3} (Fig. 1a). Compared to previous years, the spatial structure of the 2020 SEMB event resembled the one that occurred in 2008 (e.g. Dilmahamod et al., 2019), albeit with much higher Chl *a* concentrations in 2020 (Fig. 1b, c). As opposed to previous years, the 2020 SEMB event started in November 2019 in the Madagascar Basin and was pronounced in two large rings with monthly mean Chl *a* concentrations reaching 1 mg m^{-3} at 25° S, 52° E (Fig. S1 in the Supplement). These large Chl *a* rings were likely linked to eddies and/or to the retroflection of the South-East Madagascar Current (SEMC; Lutjeharms, 1988; Longhurst, 2001; de Ruijter et al., 2004; Ramanantsoa et al., 2021), as seen in the surface currents fields in November 2019 (Fig. S2 in the Supplement). In December 2019, the surface of the SEMB extended in all directions, and a maximum monthly mean Chl *a* concentration up to 2.9 mg m^{-3} was detected around 25° S, 51.5° E (Fig. S1). The SEMB was less developed in late February 2020 (Fig. S1). Whatever the origin and multiple drivers of the SEMB in 2020 through internal or external forcing (Dilmahamod et al., 2019), this rather strong biological event would significantly draw down the C_T concentration and fCO_2 during several weeks from November 2019 to February 2020 in this region.

Along the OISO-30 cruise track at 54° E in January 2020, the underway surface measurements started at 26.5° S for fCO_2 and at 27° S for A_T and C_T. Along this track the sea surface Chl *a* concentrations were relatively lower south of 27° S (0.2–0.4 mg m^{-3}) than north of 27° S (0.8–1.2 mg m^{-3}, Fig. 3a). This was associated with a rapid decrease in fCO_2 (Fig. 3a) and salinity-normalized C_T (N-$C_T = C_T \times 35/SSS$) concentration (Fig. 3b). Because there was a sharp gradient in salinity at that latitude (Fig. S3 in the Supplement), no significant change was observed for salinity-normalized A_T (N-$A_T = A_T \times 35/SSS$) along the track (Fig. 3b). The structure of the currents from November 2019 to January 2020 (Figs. S2 and S4 in the Supplement) suggests that the extension of the bloom was linked to the retroflection of the SEMC occurring around 24–26° S, one of the forms of the SEMC retroflection defined by Ramanantsoa et al. (2021) that would transport nutrients eastward in the Indian Ocean. The current field in January 2020 presents a complex meandering structure deflecting southward at 51° E and recirculating northward around 53° E (Fig. S4). Further east, at 54° E along the cruise track, the ADCP data recorded during the OISO-30 cruise revealed the presence of a relatively strong westward current (up to 40 cm s^{-1}) centred around 28–29° S identified down to 600 m. As opposed to the SEMC retroflection, this westward current would bring high salinity and low nutrients from the subtropics.

The mean properties and differences within and out of the peak bloom are listed in Table 1. Although the ocean was warmer in the bloom at 27° S (about +1 °C, Fig. S3), fCO_2 was clearly much lower at that location. The fCO_2 difference within and out of the peak bloom was −33 µatm based on fCO_2 measurements. Given the error associated with the fCO_2 calculations using A_T and C_T data (±13 µatm, Orr et al., 2018), the observed fCO_2 difference is confirmed with fCO_2 calculated with the A_T–C_T pairs (difference of −34.5 µatm, last column in Table 1). If one takes into account the effect of the warming on fCO_2 (Takahashi et al., 1993), the fCO_2 in the bloom would be 323.5 µatm. Therefore the sole impact of the biological processes in the bloom reduced fCO_2 by −49.3 µatm. This is a very large effect and coherent with the observed difference in N-C_T of −23.4 µmol kg^{-1} within and out of the bloom and almost no change in N-A_T (Table 1).

The atmospheric xCO_2 was 410 ppm in January 2020, equivalent to 397 µatm for fCO_2^{atm} (dashed line in Fig. 3a, where xCO_2 in ppm was corrected to fCO_2 according to Weiss and Price, 1980). Consequently the region was a strong CO_2 sink within the bloom area with a maximal ΔfCO_2 value of −60 µatm at 27° S (where $\Delta fCO_2 = fCO_2^{oce}$-$fCO_2^{atm}$). As a comparison at this location (28–24° S, 52.5° E), the climatological ΔfCO_2 value for January (Takahashi et al., 2009) was estimated between +4 and +10 µatm, i.e. a small source or near equilibrium. It is well known that gas exchange at the air–sea interface depends on both ΔfCO_2 and the wind speed (e.g. Wanninkhof, 2014). The net flux of CO_2 across the air–sea interface (FCO_2) was calculated according to Eq. (1) as

$$FCO_2 = k\ K_0\ \Delta fCO_2, \quad (1)$$

where K_0 is the solubility of CO_2 in seawater calculated from in situ temperature and salinity (Weiss, 1974) and k (cm h^{-1}) is the gas transfer velocity expressed from the wind speed U (m s^{-1}) (Wanninkhof, 2014) and the Schmidt number Sc (Wanninkhof, 1992) following Eq. (2) as

$$k = 0.251U^2(Sc/660)^{-0.5}. \quad (2)$$

In the region 25–30° S, 45–60° E the average monthly wind speed (GMAO, 2015) was 7.9 m s^{-1} in January 2020. This value is the same as derived from 6 h wind speed products at 27° S, 54° E, 7.8 (±2.3) m s^{-1} (Fig. S5a in the Supplement). Using Eqs. (1) and (2), this leads to a CO_2 sink of −6.9 mmol m^2 d^{-1} at 27° S in January 2020, whereas in the climatology (Takahashi et al., 2009) this region was a CO_2 source of +0.72 mmol m^2 d^{-1} in January. In the band 26–30° S, where Chl *a* varied between 1.2 and 0.2 mg m^{-3} (Fig. 3), the CO_2 sink was still significant on average, −4.3 (±1.3) mmol m^2 d^{-1}.

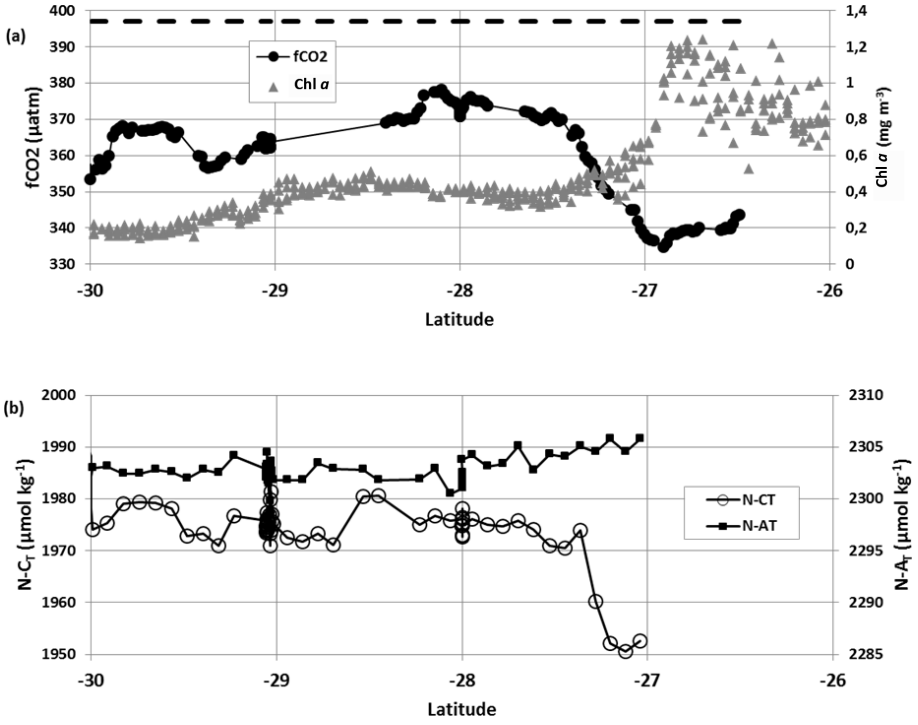

Figure 3. (a) Sea surface fCO_2 (µatm) measured in January 2020 (black circles) and Chl a (mg m^{-3}) from MODIS (4 km× 4 km) along the cruise track (grey triangles). **(b)** Sea-surface-salinity-normalized C_T (N-C_T, open circles) and salinity-normalized A_T (N-A_T, black squares) measured in January 2020 (both in µmol kg^{-1}). Low fCO_2 and N-C_T concentrations recorded around 27° S were linked to high Chl a (up to 1.2 mg m^{-3}) in the SEMB. In panel **(a)** the dashed line represents the average atmospheric fCO_2 for January 2020.

Table 1. Mean properties and their difference observed in January 2020 within and out of the SEMB peak bloom. For fCO_2, results based on measurements ($fCO_{2_{mes}}$) or calculated using A_T–C_T pairs ($fCO_{2_{cal}}$) are both listed. Standard deviations are indicated in brackets. PSU: practical salinity unit.

Region	SST °C	SSS PSU	Chl a mg m^{-3}	C_T µmol kg^{-1}	N-C_T µmol kg^{-1}	A_T µmol kg^{-1}	N-A_T µmol kg^{-1}	$fCO_{2_{mes}}$ µatm	$fCO_{2_{cal}}$ µatm
Within peak bloom (around 27° S)	26.39 (0.21)	35.22 (0.05)	0.97 (0.18)	1958.6 (2.5)	1951.7 (1.0)	2313.5 (2.7)	2305.4 (0.7)	339.5 (2.5)	329.8 (2.0)
South of the peak bloom (around 28° S)	25.32 (0.10)	35.48 (0.03)	0.41 (0.04)	2000.6 (2.2)	1975.2 (1.4)	2332.1 (1.9)	2302.4 (1.3)	372.8 (2.2)	364.3 (2.6)
Difference of in to out	+1.07	−0.26	+0.56	−42.0	−23.4	−18.6	+3.0	−33.3	−34.5

Integrated over 1 month and a surface of the bloom of 3000 km × 1500 km (Longhurst, 2001), i.e. 4.5×10^6 km^2, the carbon uptake in January 2020 would be −7.2 (±2.2) TgC per month. However, based on the Chl a distribution in January 2020 (Fig. 1a), we estimated the surface of the bloom east of 45° E to range between 1×10^6 and 1.7×10^6 km^2 depending on the criteria based on Chl a concentrations (respectively Chl $a = 0.16$ mg m^{-3} for a major bloom or Chl $a = 0.07$ mg m^{-3} for a bloom, Dilmahamod et al., 2019). This leads to an integrated CO_2 sink ranging between −1.7 and −2.7 TgC per month, probably more realistic than when using the surface of the bloom as defined by Longhurst (2001). When restricted to the surface of the domain 25–30° S, 50–60° E (0.6×10^6 km^2) the integrated CO_2 sink in January 2020 based on fCO_2 observations would be −1.0 TgC per month.

Given the fCO_2 distribution observed in January 2020 and the strong CO_2 sink evaluated within the SEMB, we then compared the 2020 observations with a period when the bloom was absent (or small) and for which fCO_2 data were also available for comparison.

4.2 Comparison with a low bloom year, 2005

For the period 1998–2016, Dilmahamod et al. (2019) synthesized the season and years (their Table 1) with strong

or moderate SEMB and years when no bloom was clearly observed, such as in 2005. This is confirmed from the Chl *a* time series constructed around 27° S that showed low Chl *a* in 2005 compared to 2004 and 2006 (Fig. 1b, c). However, it is worth noting that Poulton et al. (2009) and Srokosz and Quartly (2013) analysed in situ observations collected in this region in February 2005 during the MadEx cruise. They detected that the bloom was present, albeit with low Chl *a* concentrations (maximum of $0.2\,mg\,m^{-3}$). Based on surface observations (Chl *a*, species and nutrients) along a north-east–south-east transect between 47 and 51° E, Srokosz and Quartly (2013) reported that Chl *a* variability around 50° E was strongly linked to the eddy field as first noticed by Longhurst (2001). They also observed from SeaSoar fluorimeter data that the deep chlorophyll maximum (DCM) around 70–100 m was relatively homogenous along the cruise track and not associated with the eddy field as opposed to surface Chl *a*. Except for silicate that showed some low "patchy" concentrations ($<1\,\mu mol\,kg^{-1}$) associated with filaments of higher Chl *a* in the Madagascar Basin (Poulton et al., 2009), no significant variation was observed for other nutrients during MadEx in February 2005, and this was probably the case for fCO_2.

Here we revisited the SEMB in austral summer 2005 using data collected during the OISO-12 cruise (expocode 35MF20050113 in the SOCAT data product, Bakker et al., 2016). To compare with 2020, we selected the fCO_2 data collected along the same track around 54° E in February 2005 (note that the fCO_2 data collected in January 2005 to the east, around 60° E, were almost the same, not shown). In the region east of Madagascar, the bloom was discernible around 25° S in January 2005 with maximum Chl *a* concentrations around $0.3\,mg\,m^{-3}$ at 50° E (Fig. S6 in the Supplement). In January, the bloom appeared to extend eastward following a large meandering structure around 25° S, and in February 2005 the bloom is even detectable at 65–70° E, where Chl *a* concentration was on average 0.19 (±0.03) $mg\,m^{-3}$ within the core of the bloom. Interestingly this seems to be centred in the core of the SICC (Huhn et al., 2012) as revealed at 25° S by the ADCP observations obtained in 2005 along the OISO-12 cruise track as well as in surface current fields (Fig. S7 in the Supplement). Like in November 2019 (Fig. S2), there was a clear signal of the SEMC retroflection in January 2005 that could explain the structure and eastward propagation of the bloom. The retroflection located around 26° S, 48° E in 2005 is close to the location of the so-called "early retroflection" defined by Ramanantsoa et al. (2021) as opposed to the canonical retroflection of the SEMC found at the southern tip of Madagascar. The early retroflection of the SEMC would import nutrient-rich water from the coast in the Madagascar Basin and trigger the phytoplankton bloom.

The bloom in 2005 was low (Srokosz and Quartly, 2013; Dilmahamod et al., 2019), and thus it had no impact on the fCO_2 distribution. This is shown in Fig. 4, where we compared fCO_2 observations along the same track in February 2005 and January 2020. We present the results for ΔfCO_2 along with sea surface Chl *a* for each period. In 2005 the sea surface fCO_2 was pretty homogeneous with values near the atmospheric fCO_2 level (ΔfCO_2 values close to 0). Although one would expect to observe higher fCO_2 15 years later due to anthropogenic carbon uptake by the ocean driven by the increase in atmospheric CO_2 (and thus about the same ΔfCO_2), both fCO_2 and ΔfCO_2 in 2020 were much lower than in 2005, especially north of 27° S (Fig. 4, Table 2). In austral summer 2005, the region was near equilibrium with a ΔfCO_2 mean value of $+8.6$ (±7.1) µatm. This is close to the climatology constructed for a reference year of 2005 (Table 2 of Takahashi et al., 2014), and this is expected as the climatology included the fCO_2 data from OISO cruises obtained in this region in 1998–2008. Oppositely, in January 2020 we observed a strong sink (maximum ΔfCO_2 of -60 µatm at 27° S). As the temperature was about the same for both periods, the difference in fCO_2 was not due to thermodynamics, and the CO_2 sink observed in 2020 was directly linked to the strong SEMB that occurred in austral summer.

The average monthly wind speed was also about the same in 2020 ($7.9\,m\,s^{-1}$) and 2005 ($8.5\,m\,s^{-1}$) (Fig. S5b). Consequently the difference in the air–sea CO_2 flux between the two periods was controlled by ΔfCO_2. In the region 26–30° S, 55° E, the mean CO_2 flux in 2005 was estimated at $+1.2\,mmol\,m^{-2}\,d^{-1}$ (a source) compared to $-4.3\,mmol\,m^{-2}\,d^{-1}$ (a sink) in 2020.

5 Discussion

5.1 A large biologically driven fCO_2 negative anomaly in 2020 relative to the anthropogenic uptake of CO_2

Like for fCO_2, the N-C_T concentrations observed in the SEMB in January 2020 ($1950\,\mu mol\,kg^{-1}$, Fig. 3b, Table 1) were low compared to the climatology (Takahashi et al., 2014). At 24–28° S, 54° E, the N-C_T climatological value in January ranged between 1970 and $1980\,\mu mol\,kg^{-1}$. As the climatology produced by Takahashi et al. (2014) was referred to the nominal year of 2005, one would expect to observe higher N-C_T concentrations in 2020 due to anthropogenic CO_2 uptake.

In the Indian Ocean the decadal change of anthropogenic CO_2 (C_{ant}) was first evaluated by Peng et al. (1998) comparing data obtained in 1978 and 1995 north of 20° S. For the upper layer in the tropics (20–10° S), Peng et al. (1998) estimated an increasing rate of C_{ant} of around $1.1\,\mu mol\,kg^{-1}\,yr^{-1}$. More recently, Murata et al. (2010) evaluated the changes of C_{ant} concentrations between 1995 and 2003 in the subtropics of the southern Indian Ocean. They estimated a mean increase of C_{ant} of $+7.9$ (±1.1) $\mu mol\,kg^{-1}$ over 8.5 years in the upper layers, corresponding to a

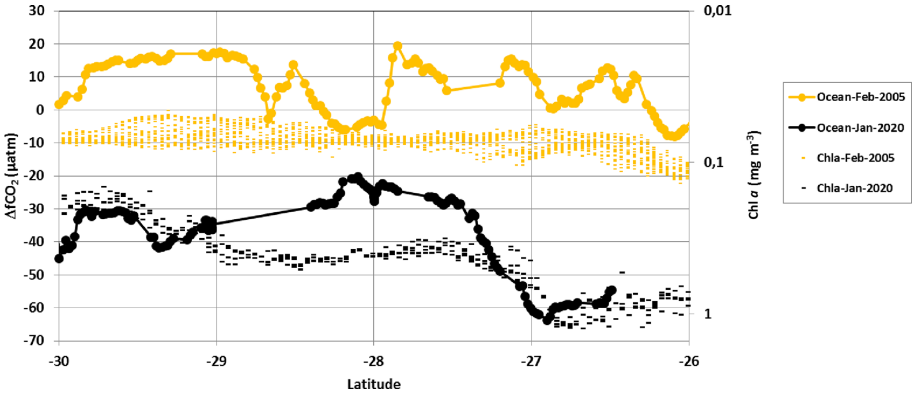

Figure 4. ΔfCO_2 (µatm) ($\Delta fCO_2 = fCO_2^{oce} - fCO_2^{atm}$) and sea surface Chl *a* (mg m^{-3}) distribution in January 2020 (black) and February 2005 (orange) along the same track around 54° E in the south-western Indian Ocean. Here Chl *a* is in $\log_{10}$ scale and inverted. In 2020 when the SEMB was particularly strong, ΔfCO_2 was negative (ocean CO_2 sink), whereas in 2005 when the bloom was small, ΔfCO_2 was close to 0 or positive (ocean CO_2 source).

Table 2. Mean sea surface properties observed along the same track in January 2020 and February 2005 in the region 30–26° S, 54° E. Also indicated are the mean values in the same region and season from the climatology of Takahashi et al. (2014) and the Chl *a* climatology evaluated for January–February 1998–2019. The number of observations for SST, SSS and fCO_2 is indicated. Standard deviations are indicated in brackets.

Cruise	Period	SST (°C)	SSS (PSU)	fCO_2 (µatm)	ΔfCO_2 (µatm)	Chl *a* (mg m^{-3})
OISO-12 115 observations	February 2005	25.443 (0.813)	35.240 (0.112)	374.2 (7.1)	+8.6 (7.1)	0.087 (0.014)
OISO-30 217 observations	January 2020	25.103 (0.739)	35.442 (0.110)	362.2 (10.7)	−36.2 (10.7)	0.489 (0.266)
Climatology	January–February	26.242 (0.898)	35.230 (0.140)	376.1 (3.6)	+10.5 (3.6)	0.105 (0.093)

trend of +0.93 (±0.13) µmol kg^{-1} yr^{-1}. In a global context, Gruber et al. (2019a, b) estimated an accumulation of anthropogenic CO_2 (C_{ant}) of +14.3 (±0.3) µmol kg^{-1} in surface waters of the south-western Indian Ocean over 1994–2007, corresponding to an increasing rate in C_{ant} of +1.10 (±0.02) µmol kg^{-1} yr^{-1}. To confirm these C_{ant} trends that were based on the C_{ant} differences between two periods (1995–1978, 2003–1995 or 2007–1994), we calculated the C_{ant} concentrations and long-term trend using water column data available in 1978–2020 in the region 30–26° S, 55° E. We extracted the data from the most recent GLODAP (Global Ocean Data Analysis Project) quality-controlled data product (GLODAPv2.2021, Lauvset et al., 2021a, b), completed with data from OISO cruises in 2012–2018. To calculate C_{ant} we used the TrOCA (Tracer combining Oxygen, inorganic Carbon, and total Alkalinity) method developed by Touratier et al. (2007). Because indirect methods are not suitable for evaluating C_{ant} concentrations in surface waters due to gas exchange and biological activity, we selected the data in the layer 100–250 m below the DCM. C_{ant} concentrations were calculated for each sample in that layer and then averaged for each period to estimate the trend (Fig. 5). As expected the C_{ant} concentrations in the subsurface increased significantly from 1978 to 2020, and the long-term trend of +1.05 (±0.08) µmol kg^{-1} yr^{-1} over this period is close to previous estimates based on different periods and approaches (Peng et al., 1998; Murata et al., 2010; Gruber et al., 2019a).

Furthermore the C_{ant} trend of around +1 µmol kg^{-1} yr^{-1} is coherent with an increase in C_T of between +0.93 and +1.17 µmol kg^{-1} yr^{-1} derived from the oceanic fCO_2 increase over the period 1991–2007 estimated from winter and summer fCO_2 data (+1.75 and +2.2 µatm yr^{-1} respectively, Metzl, 2009) assuming constant alkalinity and temperature. With the new data available after 2007, we have revisited the fCO_2 long-term trend by selecting only the austral summer data in the region around 27° S, 55° E (Fig. 2). For the period 1991–2019 we estimated an fCO_2 trend of +1.55 (±0.40) µatm yr^{-1}. This is less than the atmospheric fCO_2 increase of +1.89 (±0.03) µatm yr^{-1} over the same period, suggesting that the CO_2 sink increased at this location. In a broader context, Landschützer et al. (2016) sug-

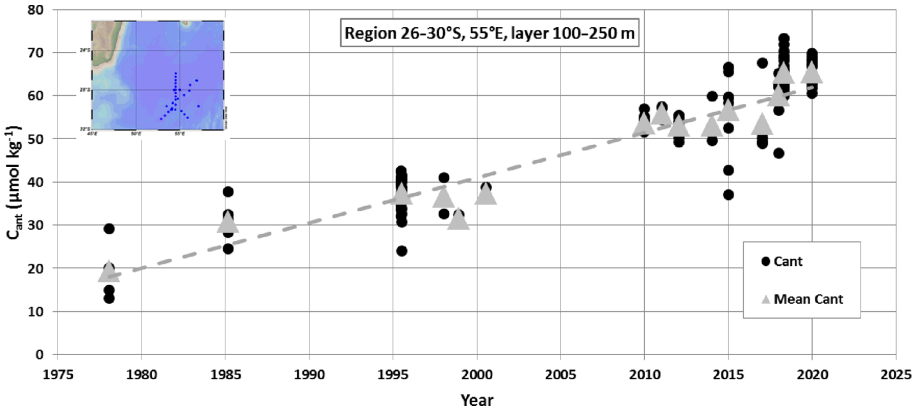

Figure 5. Time series of anthropogenic CO_2 concentrations (C_{ant}) estimated in the subsurface (layer at 100–250 m) in the region 26–30° S, 55° E from the GLODAPv2.2021 data product (Lauvset et al., 2021a, b) completed with OISO cruises in 2012–2018 (location of selected stations in the insert map). The figure shows the C_{ant} concentrations calculated for each sample (black dots) and the C_{ant} averaged in the layer at 100–250 m for each period (grey triangles). Over the period 1978–2020, the C_{ant} long-term trend is $+1.05$ (± 0.08) µmol kg^{-1} yr^{-1} (dashed grey line).

gested that the carbon uptake tended to increase slightly in 1998–2011 in the subtropical Indian Ocean (their Fig. 3). We will see that such a change in the CO_2 fluxes in this region is also revealed in the CMEMS-LSCE-FFNN model (Chau et al., 2022). Note that if at 27° S, 55° E (Fig. 2) the ocean fCO_2 data in 2020 were also used to estimate the trend (1991–2020), the rate of fCO_2 would be only $+1.09$ (± 0.48) µatm yr^{-1}, i.e. about half the atmospheric fCO_2 trend. The fCO_2 observations in 2020 represent a large negative anomaly at the local scale, and thus caution is needed when incorporating such an anomaly to detect and interpret long-term change in the CO_2 sink, at least in the south-western subtropical Indian Ocean.

To compare the fCO_2 trends listed above with the anthropogenic rate of around $+1.0$ µmol kg^{-1} yr^{-1} (Fig. 5), we have calculated C_T from the fCO_2 data and A_T derived from salinity (described below). For this calculation we used the CO2SYS programme (CO2SYS_v2.5, Orr et al., 2018) developed by Lewis and Wallace (1998) and adapted by Pierrot et al. (2006) with K_1 and K_2 dissociation constants from Lueker et al. (2000) and the KSO_4 constant from Dickson (1990). The total boron concentration is calculated according to Uppström (1974). For nutrients we fixed phosphate concentrations at 0 and silicate at 2.0 (± 0.6) µmol kg^{-1} (the mean of 79 surface observations measured during previous OISO cruises in the region 22–30° S). To derive A_T from salinity we used the surface A_T observations obtained since 1998 in the subtropical south-western Indian Ocean (OISO cruises). From these data we estimated a robust relationship (Fig. 6):

$$A_T\left(\mu\text{mol kg}^{-1}\right) = 62.1601 \cdot \text{SSS} + 123.1$$
$$\left(\text{rms} = 7.0\ \mu\text{mol kg}^{-1}, r = 0.89, n = 3400\right). \quad (3)$$

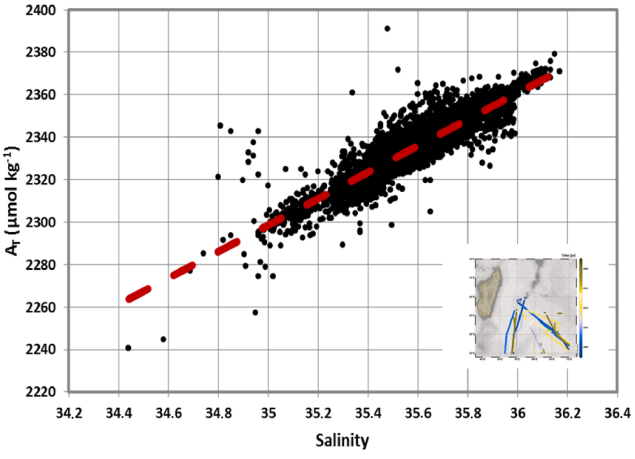

Figure 6. Relationship of A_T (µmol kg^{-1}) versus salinity deduced from surface A_T data ($n = 3400$) obtained during OISO cruises in 1998–2020 in the south-western Indian Ocean. For the subtropics we have selected the data in the region 35–20° S, 50–70° E (track of cruises shown in the insert map). The relationship (red dashed) is $A_T = 62.1601 \cdot \text{SSS} + 123.1$ and is used to calculate C_T concentrations in this region (Fig. 7). A_T data are available at NCEI OCADS (https://www.ncei.noaa.gov/access/ocean-carbon-data-system/oceans/VOS_Program/OISO.html, last access: 3 March 2022).

The use of other relationships (e.g. Millero et al., 1998; Lee et al., 2006) would slightly change the A_T concentrations but not the interpretation on the C_T trend in this region. The time series of salinity-normalized C_T (N-$C_T = C_T \times 35/\text{SSS}$) at 27–28° S, 55° E shows that N-C_T increased over the period 1991–2019 at a rate of $+0.70$ (± 0.24) µmol kg^{-1} yr^{-1} (Fig. 7). This is somehow lower than the anthropogenic trend of $+1$ µmol kg^{-1} yr^{-1}, suggesting that in addition to the anthropogenic CO_2 uptake,

natural processes could also have a small impact on the C_T and fCO_2 trends in surface waters over almost 30 years.

Having an estimate of the C_T change due to anthropogenic CO_2 (around $+1\,\mu mol\,kg^{-1}\,yr^{-1}$) and taking into account this effect, the climatological N-C_T concentration of $1973\,\mu mol\,kg^{-1}$ for 2005 (Takahashi et al., 2014) corrected for the year 2020 would be $1988\,\mu mol\,kg^{-1}$ in the region of interest. This is higher by up to $+36\,\mu mol\,kg^{-1}$ than the observed N-C_T in January 2020 in the SEMB (Table 1, Fig. 7). When correcting the climatological value to the observed C_T trend of $+0.7\,\mu mol\,kg^{-1}\,yr^{-1}$, the N-C_T in 2020 would be $1983.5\,\mu mol\,kg^{-1}$, i.e. $+32.5\,\mu mol\,kg^{-1}$ higher than the observed value in January 2020. The N-C_T anomaly in January 2020 is also large compared to the mean N-C_T seasonal amplitude of $20\,\mu mol\,kg^{-1}$ generally observed in the subtropics of the southern Indian Ocean (Metzl et al., 1998; Takahashi et al., 2014). We also note that climatological N-A_T concentrations of $2295\,\mu mol\,kg^{-1}$ for January (Takahashi et al., 2014) are very close to those we observed in January 2020 (Table 1, Fig. 3b). Therefore the low fCO_2 and strong CO_2 sink in 2020 in the SEMB is due to a large drawdown of C_T, i.e. not driven by temperature changes or alkalinity.

5.2 Specificities of the SEMB in 2020

Based on previous studies it is likely that the biologically driven reduction of C_T in the SEMB under depleted sea surface nitrate concentrations was associated with the process of N_2 fixation (Uz, 2007). The hypothesis that diazotrophy would play a role in the temporal C_T (and thus fCO_2) variability is supported by the observation of large N_2-fixing phytoplankton in the SEMB region in 2005 during the MadEx cruise (Poulton et al., 2009). These authors found that the filamentous cyanobacteria *Trichodesmium* was most abundant south of Madagascar (over the Madagascar Ridge), whereas diatom–diazotroph associations (such as *Rhizosolenia–Richelia*) were mainly observed east of Madagascar (in the Madagascar Basin).

Our measurements in January 2020 showed high spatial variability of the N_2 fixation rate (range from 0.8 to $18.3\,nmol\,N\,L^{-1}\,d^{-1}$, Fig. 8). Such variability in the subtropical Indian Ocean was also recently reported by Hörstmann et al. (2021), who measured N_2 fixation rates between 0.7 and $7.9\,nmol\,N\,L^{-1}\,d^{-1}$ in January–February 2017 in the same region (OISO-27 cruise) but when the SEMB was not pronounced (Fig. 1b, c) and when fCO_2 was high and above equilibrium (Fig. 2). Our results for silicate (Si) and N_2 fixation observations are difficult to interpret because few samples were collected along the track (Fig. 8). A maximum of the N_2 fixation rate was observed at 30° S that was not linked to changes in other properties. This local high N_2 fixation rate could be related to *Trichodesmium* species, but it was not sampled in January 2020. We also noted low Si concentrations at 27° S ($0.6\,\mu mol\,kg^{-1}$) associated with higher Chl *a* and lower fCO_2 and C_T (Fig. 3). The low silicate might be associated with the presence of diatom–diazotroph associations (DDAs) as observed during the MadEx cruise (Poulton et al., 2009). In the bloom, N_2 fixation increased northward from 28° S (factor of ~ 5). Based on measurements for different size fractions we observed that the N_2 fixation is mainly related to the fraction $>20\,\mu m$ (i.e. *Trichodesmium* and DDA) representing 88 % (±9 %) of the N_2 fixation. "Hotspots" of large diazotrophs (20–180 and 180–2000 µm) were also detected in other regions of the south-western Indian Ocean in May 2010 during the *Tara* expedition (Pierella Karlusich et al., 2021).

At a global scale, the presence of N_2 fixers in the south-western Indian Ocean has been detected from satellite data (Westberry and Siegel, 2006; Qi et al., 2020), and relatively high N_2 fixation rates in austral summer in this region were also derived from N_2 fixation data using a machine learning approach (Tang and Cassar, 2019; Tang et al., 2019). A large-scale distribution of diazotrophy was further estimated from surface C_T observations, suggesting the presence of N_2 fixers in the Mozambique Channel and the south-western Indian Ocean (Lee et al., 2002; Ko et al., 2018). These authors used regional relationships of N-C_T versus SST to reconstruct the N-C_T field from which they estimated the net carbon production (NCP) in nitrate depleted waters, a proxy for carbon production by N_2-fixing microorganisms. The N-C_T–SST relationship observed from in situ data in January 2020 somehow mimics this process (Fig. 9); i.e. the inter-annual variability of the N-C_T–SST relationship would also inform the NCP by N_2 fixers.

Sea surface warming and shallow mixed-layer depth (MLD) are proposed to lead to optimal conditions for the growth of the N_2 fixers and generate the SEMB (e.g. Longhurst, 2001; Srokosz et al., 2015). In austral summer 2020, the ocean was not much warmer than previous years, suggesting that temperature was not a specific driver of the SEMB that year. To the contrary, in January 2020 the region experienced a particularly shallow MLD which might have favoured the bloom (observed MLD around 20 m at 27–28° S, Figs. S8 and S9 in the Supplement).

As noted above, the strong bloom started in November 2019 and could be well identified in two large rings (Fig. S1). In the northern ring at 25° S, 52° E, the MLD was deep (>80 m) during 3 consecutive months in July–September 2019 and deeper compared to previous years (Fig. S10 in the Supplement). This would have injected nutrients (and maybe iron) in surface layers, and when the MLD was shallow at that location (<20 m) the bloom developed in November 2019 and reached high Chl *a* values in December 2019 (up to $1.8\,mg\,m^{-3}$). As the bloom covered a large region in December 2019 and January 2020, other specific processes like iron supply (from dust, coastal zone, rivers or sediments) still need to be identified to fully explain 2020 SEMB dynamics. The 2020 bloom was clearly recognized in Chl *a*, fCO_2 and C_T observations, but at that stage we have

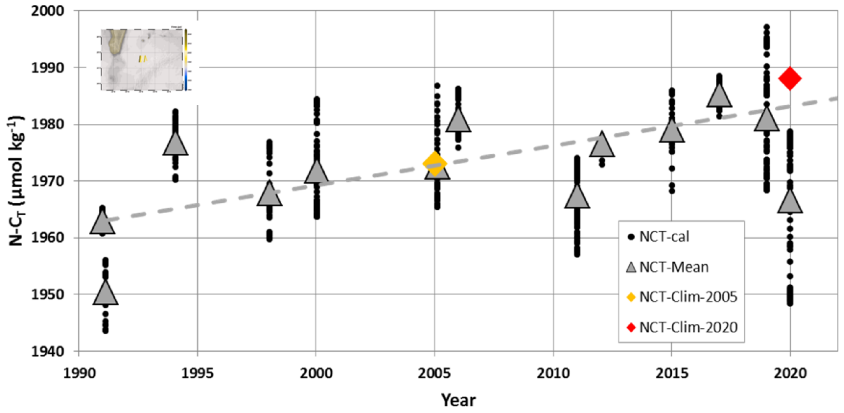

Figure 7. Time series of salinity-normalized C_T (N-C_T, black dots) and their monthly mean (grey triangles) at 27–28° S, 55° E (insert map) calculated with fCO_2 observations (see Fig. 2) and reconstructed A_T from salinity (Fig. 6). The figure shows data for the months of January and February (data available from 1991 to 2020 for austral summer). Over the period 1991–2019, the N-C_T trend is $+0.70$ (± 0.24) µmol kg^{-1} yr^{-1} (dashed grey line), reflecting in part the anthropogenic CO_2 uptake. Note the low N-C_T in January 2020 in the SEMB compared to previous years with some values around 1950 µmol kg^{-1} in 2020 as low as N-C_T calculated in 1991. The N-C_T concentration in the same region derived from the climatology of Takahashi et al. (2014) is also plotted (orange diamond for the reference year of 2005) as well as the climatological value for the year 2020 after correcting for anthropogenic CO_2 (red diamond).

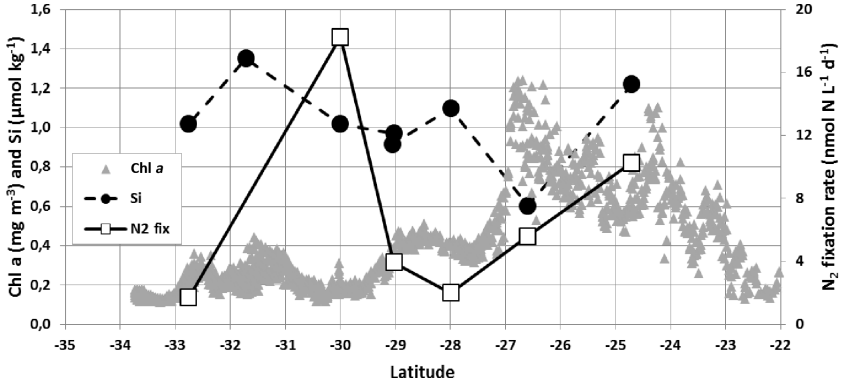

Figure 8. Sea surface silicate concentration (Si, µmol kg^{-1}, black circles, scale on the left), N_2 fixation rate (N_2 fix, nmol N L^{-1} d^{-1}, open squares, scale on the right) measured in January 2020 (OISO-30 cruise) and Chl a (mg m^{-3}, grey triangles, scale on the left) from MODIS (4 km × 4 km) along the cruise track. The low Si concentration (0.6 µmol kg^{-1}) recorded around 27° S was linked to higher Chl a (up to 1.2 mg m^{-3}) in the SEMB.

no clear explanation on the process (or multiple drivers) that generated its extent and intensity.

5.3 The changing ocean CO_2 uptake in the SEMB based on reconstructed pCO_2

The results presented above were based on local underway fCO_2 observations, and the integrated air–sea CO_2 fluxes were thus extrapolated from local data on a surface representing the area covered by the bloom leading to a carbon uptake of between −1.7 and −2.7 TgC per month in January 2020. In the domain 25–30° S, 50–60° E we estimated a CO_2 sink in January 2020 close to −1 TgC per month.

To evaluate the impact of the bloom at the regional scale, we used monthly surface ocean pCO_2 and air–sea CO_2 flux fields reconstructed by a neural network method as described in Sect. 3 (CMEMS-LSCE-FFNN, Chau et al., 2022). The SEMB was well developed in December 2019, and we can evaluate its impact on the air–sea CO_2 fluxes by comparing December 2018 (low bloom) and December 2019 (strong bloom, Fig. 10). In the region 25–30° S, 50–60° E, the average pCO_2 in December 2019 (375.9 ± 6.3 µatm) was much lower than in December 2018 (396.6 ± 6.0 µatm) and thus opposite of the expected pCO_2 increase due to anthropogenic CO_2 uptake. At the local scale, within the bloom at 27° S, 54° E or at 29° S, 50° E, the CMEMS-LSCE-FFNN model estimated low pCO_2 clearly linked to higher Chl a in December 2019 (Figs. S11 and S12 in the Supplement). Consequently the region was a small CO_2 source of $+0.07$ (± 0.53) mmol m^{-2} d^{-1} in December 2018 but a CO_2

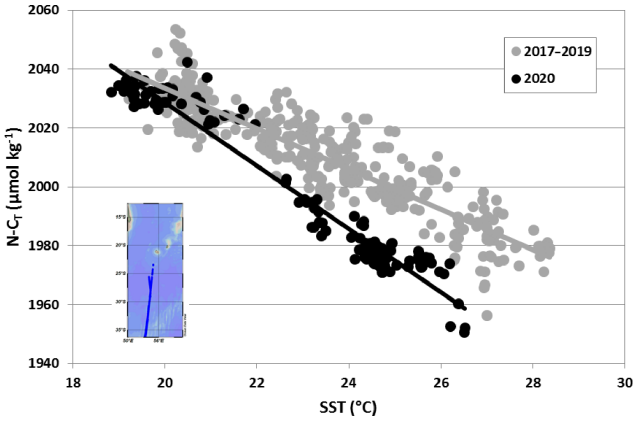

Figure 9. The relationship between N-C_T (µmol kg^{-1}) and SST in surface waters based on OISO cruises observations in the south-western Indian Ocean in austral summer 2017, 2018, 2019 and 2020 along the same repeated track (insert map). In January 2020 during the strong SEMB, the N-C_T–SST relationship (black dots and black line) was much sharper than in 2017–2019 (grey dots and grey line), indicative of N_2 fixation production in nitrate depleted waters (e.g. Ko et al., 2018).

sink in December 2019 of -3.1 (± 1.0) mmol m^{-2} d^{-1}. Integrated over the region 25–30° S, 50–60° E the carbon uptake changed from a small CO_2 source in December 2018 of $+0.019$ TgC per month to a CO_2 sink in December 2019 of -0.8 TgC per month (Fig. S13 in the Supplement), close to the estimate derived from observations in January 2020 (-1.0 TgC per month). Over the period 1996–2018, each year the model evaluates a CO_2 source in December averaging $+0.12$ (± 0.10) TgC per month. This suggests that in late 2019 the CMEMS-LSCE-FFNN model did capture the effect of the SEMB on pCO_2 and CO_2 fluxes, leading to a stronger regional CO_2 annual sink in 2019 (-8.8 TgC yr^{-1}) compared to previous years (Fig. 11). A major SEMB was previously recognized in 1999, 2006 and 2008 (Dilmahamod et al., 2019; see also Fig. 1). The model overestimates the CO_2 sink in 2006 and 2008 but surprisingly not in 1999 (Fig. 11). This is probably because the ocean was warmer from December 1998 to March 1999, inducing a positive anomaly of fCO_2 that would balance the decrease of fCO_2 due to the biological activity in summer 1999. With the exception of 2008 when the SEMB was also strong (Fig. 1), the CO_2 sink anomalies in 1998–2018 appeared relatively modest compared to that observed in 2019 (Fig. 11).

6 Conclusions

The new observations in the south-western Indian Ocean presented here showed that the fCO_2 and C_T concentrations in January 2020 have been very low and far from normal conditions since 1991. This is explained by the strong SEMB event that started in November 2019 in this region and was well developed in December 2019 and January 2020. Thanks to the continuous ocean colour satellite data since 1997, the time series of Chl a in this region showed that the bloom was particularly strong in austral summer 2019/20. We suspect that prior to 1997, the SEMB had been less intense as suggested by in situ fCO_2 data in 1991–1994 (Fig. 2). We estimated that the SEMB led to a regional carbon uptake of between -1.7 and -2.7 TgC per month in January 2020. The variation of the regional ocean CO_2 sink due to the SEMB developed in late 2019 was also quantified with the CMEMS-LSCE-FFNN model. Model results indicate a large anomaly in December 2019 that led to an annual sink of -8.8 TgC yr^{-1}, i.e. about 1 TgC yr^{-1} larger than previous years. The strong bloom in austral summer 2020 represents an interesting benchmark case to test models for a better understanding of the origin of the SEMB and its impact on the regional ocean CO_2 sink. Future studies should target sensitivity analysis with complex biogeochemical models including the CO_2 system, at different spatial resolution for the dynamics and with (or without) N_2 fixers (e.g. Monteiro et al., 2010; Landolfi et al., 2015; Paulsen et al., 2017). This plankton functional type is not yet included in models dedicated to this region (Srokosz et al., 2015; Dilmahamod et al., 2020). The new fCO_2, C_T, A_T and N_2 fixation rate observations presented here along with historical data (e.g. SOCAT, Bakker et al., 2016, 2021; Fig. 2) could serve as a validation to compare periods with or without bloom. In the future, if the SEMB as observed in 2020 is more frequent or becomes a regular situation and if organic matter is exported below the surface mixed layer, this could represent a negative feedback to the ocean carbon cycle; i.e. the ocean sink would be enhanced. As already noted by several authors (e.g. Dilmahamod et al., 2019), dedicated studies in this region at the scale of eddies coupling dynamical and biological processes, including not only the sampling of plankton and nutrients (e.g. iron) but also the determination of rates (e.g. N_2 fixation), would be relevant to understanding the processes controlling the SEMB and to evaluating its impact on the biological carbon pump.

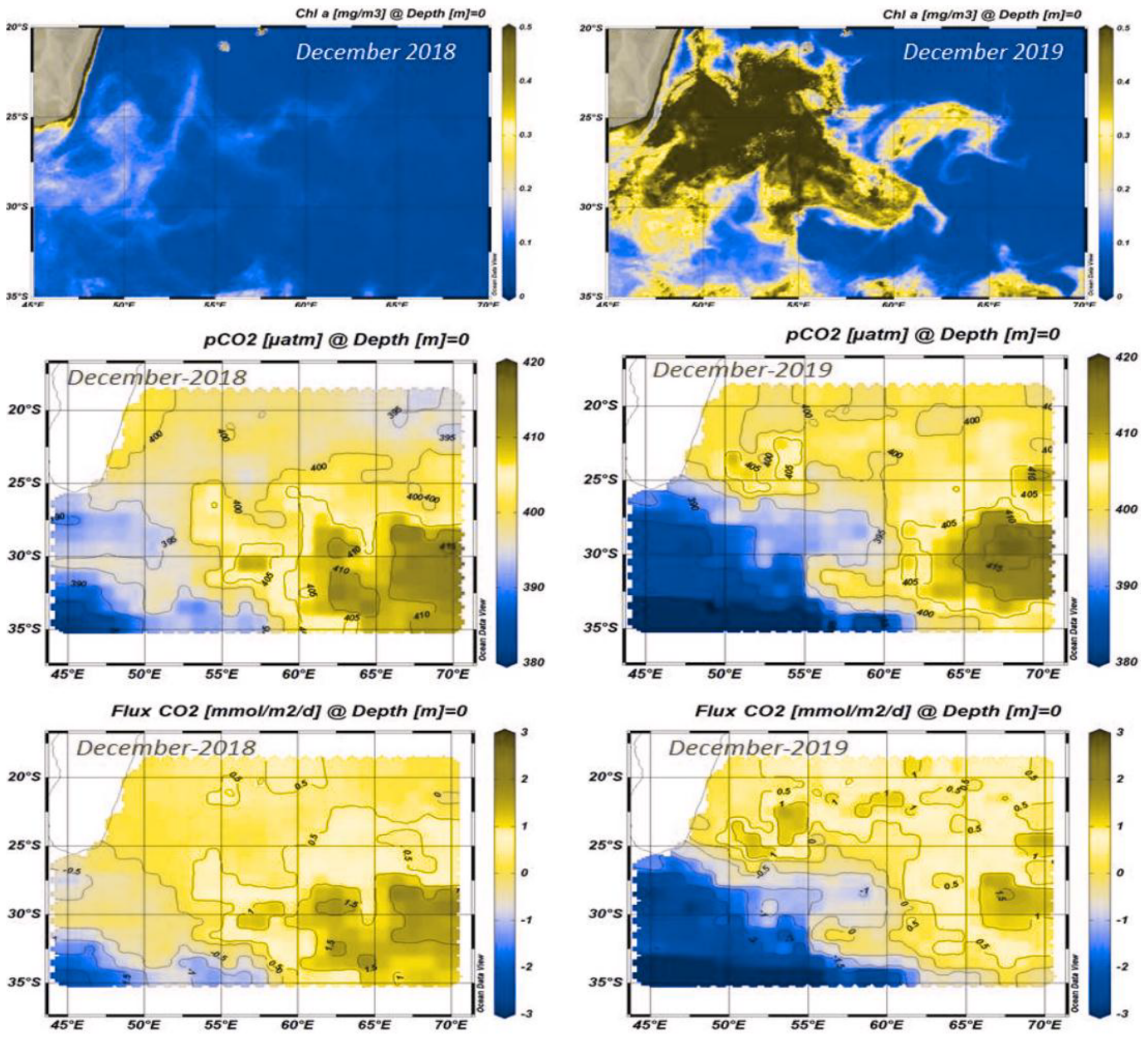

Figure 10. Maps of Chl *a* (mg m^{-3}), pCO_2 (µatm) and the air–sea CO_2 fluxes (mmol m^{-2} d^{-1}) in the south-western Indian Ocean in December 2018 (left) and December 2019 (right). In December 2019 when the SEMB was particularly strong, the pCO_2 was lower, and air–sea CO_2 fluxes were negative (ocean sink, in blue), whereas in December 2018 when the bloom was small, the fluxes were near equilibrium or positive in this region (ocean source, yellow-brown). Chl *a* data downloaded from https://resources.marine.copernicus.eu/ (OCEANCOLOUR_GLO_CHL_L4_REP_OBSERVATIONS_009_093, last access: 10 April 2021). Figures produced with ODV (Schlitzer, 2013).

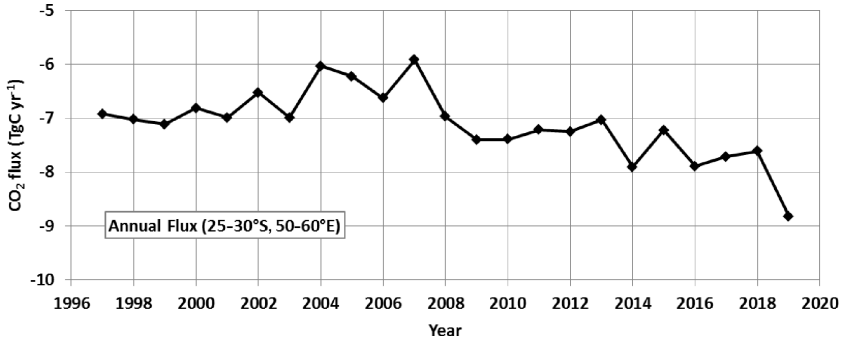

Figure 11. Annual air–sea CO_2 flux (TgC yr^{-1}) in the south-western Indian Ocean (region of 25–30° S, 50–60° E) for the period 1996–2019 from the CMEMS-LSCE-FFNN model. The carbon uptake progressively increased after 2007 with a maximum CO_2 sink estimated in 2019 when the SEMB was particularly strong.

Data availability. The SOCAT-v2021 data are available at https://www.socat.info/index.php/data-access/ (last access: 3 March 2022) and at https://doi.org/10.25921/4xkx-ss49 (Bakker et al., 2021). The GLODAPv2.2021 data are available at https://www.glodap.info/index.php/merged-and-adjusted-data-product-v22021/ (last access: 3 March 2022) and https://doi.org/10.25921/ttgq-n825 (Lauvset et al, 2021b). The OISO surface A_T–C_T data are available at https://www.ncei.noaa.gov/access/ocean-carbon-data-system/oceans/VOS_Program/OISO.html (last access: 3 March 2022). The OISO ADCP data are available at http://uhslc.soest.hawaii.edu/sadcp/DATABASE/01545.html (last access: 3 March 2022). The CMEMS-LSCE-FFNN model data are available from the Copernicus Marine Service at https://resources.marine.copernicus.eu/products (last access: 3 March 2022) and https://doi.org/10.48670/moi-00047 (Chau et al, 2020).

Supplement. The supplement related to this article is available online at: https://doi.org/10.5194/bg-19-1451-2022-supplement.

Author contributions. CLM and NM are co-investigators of the ongoing OISO project. fCO_2, A_T and C_T data for OISO-30 were measured by CLM, CL and CM and qualified by CLM and NM. Nutrient data for OISO-30 were measured and qualified by CL. N_2 fixation data for OISO-30 were measured and qualified by CR. CLM, NM and JF qualified fCO_2, A_T and C_T data for previous OISO cruises. MG and TTTC developed the CMEMS-LSCE-FFNN model and provided the model results. NM started the analysis, wrote the draft of the manuscript and prepared the figures with contributions from all authors.

Competing interests. The contact author has declared that neither they nor their co-authors have any competing interests.

Disclaimer. Publisher's note: Copernicus Publications remains neutral with regard to jurisdictional claims in published maps and institutional affiliations.

Acknowledgements. The OISO programme was supported by the French institutes INSU (Institut National des Sciences de l'Univers) and IPEV (Institut polaire français Paul-Émile Victor), OSU Ecce Terra (at Sorbonne Université), and the French programme SOERE/Great-Gases. We thank the French oceanographic fleet ("flotte océanographique française") for financial and logistic support to the OISO programme and the OISO-30 oceanographic campaign (https://doi.org/10.17600/18000679). We thank the captains and crew of RV *Marion Dufresne* and the staff at IFREMER, GENAVIR and IPEV. We thank Magloire Mandeng-Yogo and Fethiye Cetin for the measurements performed with the ALYSÉS platform (OSU Ecce Terra). The Surface Ocean CO_2 Atlas (SOCAT, http://www.socat.info/, last access: 3 March 2022) is an international effort, endorsed by the International Ocean Carbon Coordination Project (IOCCP), the Surface Ocean – Lower Atmosphere Study (SOLAS) and the Integrated Marine Biosphere Research (IMBeR) programme to deliver a uniformly quality-controlled surface ocean CO_2 database. We thank Meric Srokosz and Ahmad Fehmi Dilmahamod for their fast reviews and suggestions and the associate editor, Peter Landschützer, for managing this paper.

Financial support. This research has been supported by the Centre National de la Recherche Scientifique (SNO OISO; SOERE/Great-Gases; LEFE ITALIANO; and PPR-Green-Grog, grant no. 5-DS-PPR-GGREOG), the Sorbonne Université (SNO OISO) and the European Commission Horizon 2020 framework programme (AtlantOS, grant no. 633211).

Review statement. This paper was edited by Peter Landschützer and reviewed by Meric Srokosz and Ahmad Fehmi Dilmahamod.

References

Aminot, A. and Kérouel, R.: Dosage automatique des nutriments dans les eaux marines, Méthodes en flux continu, first edn., Ifremer-Quae, 188 pp., ISBN 13 978-2-7592-0023-8, 2007.

Bakker, D. C. E., Pfeil, B., Landa, C. S., Metzl, N., O'Brien, K. M., Olsen, A., Smith, K., Cosca, C., Harasawa, S., Jones, S. D., Nakaoka, S., Nojiri, Y., Schuster, U., Steinhoff, T., Sweeney, C., Takahashi, T., Tilbrook, B., Wada, C., Wanninkhof, R., Alin, S. R., Balestrini, C. F., Barbero, L., Bates, N. R., Bianchi, A. A., Bonou, F., Boutin, J., Bozec, Y., Burger, E. F., Cai, W.-J., Castle, R. D., Chen, L., Chierici, M., Currie, K., Evans, W., Featherstone, C., Feely, R. A., Fransson, A., Goyet, C., Greenwood, N., Gregor, L., Hankin, S., Hardman-Mountford, N. J., Harlay, J., Hauck, J., Hoppema, M., Humphreys, M. P., Hunt, C. W., Huss, B., Ibánhez, J. S. P., Johannessen, T., Keeling, R., Kitidis, V., Körtzinger, A., Kozyr, A., Krasakopoulou, E., Kuwata, A., Landschützer, P., Lauvset, S. K., Lefèvre, N., Lo Monaco, C., Manke, A., Mathis, J. T., Merlivat, L., Millero, F. J., Monteiro, P. M. S., Munro, D. R., Murata, A., Newberger, T., Omar, A. M., Ono, T., Paterson, K., Pearce, D., Pierrot, D., Robbins, L. L., Saito, S., Salisbury, J., Schlitzer, R., Schneider, B., Schweitzer, R., Sieger, R., Skjelvan, I., Sullivan, K. F., Sutherland, S. C., Sutton, A. J., Tadokoro, K., Telszewski, M., Tuma, M., van Heuven, S. M. A. C., Vandemark, D., Ward, B., Watson, A. J., and Xu, S.: A multi-decade record of high-quality fCO_2 data in version 3 of the Surface Ocean CO_2 Atlas (SOCAT), Earth Syst. Sci. Data, 8, 383–413, https://doi.org/10.5194/essd-8-383-2016, 2016.

Bakker, D. C. E., Alin, S. R., Castaño-Primo, R., Cronin, M., Gkritzalis, T., Kozyr, A., Lauvset, S. K., Metzl, N., Munro, D. R., Nakaoka, S.-I., O'Brien, K. M., Olsen, A., Omar, A. M., Pfeil, B., Pierrot, D., Rodriguez, C., Steinhoff, T., Sutton, A. J., Tilbrook, B., Wanninkhof, R., Willstrand, A., Ahmed, M., Andersson, A., Apelthun, L. B., Bates, N., Battisti, R., Beaumont, L., Becker, M., Benoit-Cattin, A., Berghoff, C. F., Boutin, J., Burger, E. F., Burgers, T. M., Cantoni, C., Cattrijsse, A., Chierici, M., Cross, J. N., Coppola, L., Cosca, C. E., Currie, K. I., De Carlo, E. H., Else, B., Enright, M. P., Ericson, Y., Evans, W., Feely, R. A., Fiedler, B., Fransson, A., García-Ibáñez, M. I., Gehrung, M., Glockzin, M., González Dávila, M., Gutekunst, S., Hermes, R., Humphreys, M. P., Hunt, C. W., Ibánhez, J. S. P., Jones, S. D., Ki-

tidis, V., Körtzinger, A., Kosugi, N., Landa, C. S., Landschützer, P., Lefèvre, N., Lo Monaco, C., Luchetta, A., Lutz, V. A., Macovei, V., Manke, A. B., Merlivat, L., Millero, F. J., Monacci, N. M., Negri, R. M., Newberger, T., Newton, J., Nickford, S. E., Nojiri, Y., Ohman, M., Ólafsdóttir, S. R., Sweeney, C., Ono, T., Palter, J. B., Papakyriakou, T., Petersen, W. T., Plueddemann, A. J., Qi, D., Rehder, G., Ritschel, M., Rutgersson, A., Sabine, C. L., Salisbury, J. E., Santana-Casiano, J. M., Schlitzer, R., Send, U., Skjelvan, I., Smith, K., Sparnocchia, S., Sullivan, K. F., Sutherland, S. C., Szuts, Z., Tadokoro, K., Tanhua, T., Telszewski, M., Theetaert, H., Vandemark, D., Voynova, Y., Wada, C., Weller, R. A., and Woosley, R. J.: Surface Ocean CO_2 Atlas Database Version 2021 (SOCATv2021) (NCEI Accession 0235360), NOAA National Centers for Environmental Information [data set], https://doi.org/10.25921/4xkx-ss49, 2021.

Bates, N. R., Pequignet, A. C., and Sabine, C. L.: Ocean carbon cycling in the Indian Ocean: 1. Spatiotemporal variability of inorganic carbon and air-sea CO_2 gas exchange, Global Biogeochem. Cy., 20, GB3020, https://doi.org/10.1029/2005GB002491, 2006.

Broullón, D., Pérez, F. F., Velo, A., Hoppema, M., Olsen, A., Takahashi, T., Key, R. M., Tanhua, T., Santana-Casiano, J. M., and Kozyr, A.: A global monthly climatology of oceanic total dissolved inorganic carbon: a neural network approach, Earth Syst. Sci. Data, 12, 1725–1743, https://doi.org/10.5194/essd-12-1725-2020, 2020.

Chau, T. T. T., Gehlen, M., and Chevallier, F.: QUALITY INFORMATION DOCUMENT for Global Ocean Surface Carbon Product MULTIOBS_GLO_BIO_CARBON_SURFACE_REP_015_008, Res. Rap. Lab. Sci. Clim. Environ., 25 [data set], https://doi.org/10.48670/moi-00047, 2020.

Chau, T. T. T., Gehlen, M., and Chevallier, F.: A seamless ensemble-based reconstruction of surface ocean pCO_2 and air–sea CO_2 fluxes over the global coastal and open oceans, Biogeosciences, 19, 1087–1109, https://doi.org/10.5194/bg-19-1087-2022, 2022.

Copin-Montégut, C.: A new formula for the effect of temperature on the partial pressure of CO_2 in seawater, Mar. Chem., 25, 29–37, https://doi.org/10.1016/0304-4203(88)90012-6, 1988.

Copin-Montégut, C.: Corrigendum, A new formula for the effect of temperature on the partial pressure of CO_2 in seawater, Mar. Chem., 27, 143–144, https://doi.org/10.1016/0304-4203(89)90034-0, 1989.

Coverly, S. C., Aminot, A., and Kérouel, R.: Nutrients in Seawater Using Segmented Flow Analysis, in: Practical Guidelines for the Analysis of Seawater, edited by: Wurl, O., CRC Press, chap. 8, 143–178, https://doi.org/10.1201/9781420073072, 2009.

Denvil-Sommer, A., Gehlen, M., Vrac, M., and Mejia, C.: LSCE-FFNN-v1: a two-step neural network model for the reconstruction of surface ocean pCO_2 over the global ocean, Geosci. Model Dev., 12, 2091–2105, https://doi.org/10.5194/gmd-12-2091-2019, 2019.

de Ruijter, W. P. M., van Aken, H. M., Beier, E. J., Lutjeharms, J. R. E., Matano, R. P., and Schouten, M. W.: Eddies and dipoles around South Madagascar: Formation, pathways and large-scale impacts, Deep-Sea Res. Pt. I, 51, 383–400, https://doi.org/10.1016/j.dsr.2003.10.011, 2004.

Dickson, A. G.: Standard potential of the reaction: $AgCl(s) + 1/2H_2(g) = Ag(s) + HCl(aq)$, and the standard acidity constant of the ion HSO_4 – in synthetic sea water from 273.15 to 318.15 K, J. Chem. Thermodyn., 22, 113–127, https://doi.org/10.1016/0021-9614(90)90074-Z, 1990.

Dilmahamod, A. F., Penven, P., Aguiar-González, B., Reason, C. J. C., and Hermes, J. C.: A new definition of the South-East Madagascar Bloom and analysis of its variability, J. Geophys. Res.-Oceans, 124, 1717–1735, https://doi.org/10.1029/2018JC014582, 2019.

Dilmahamod, A. F., Penven, P., Aguiar-Gonzalez, B., Reason, C. J. C., and Hermes, J. C.: A model investigation of the influences of the South-East Madagascar current on the South-East Madagascar bloom, J. Geophys. Res.-Oceans, 125, e2019JC015761, https://doi.org/10.1029/2019JC015761, 2020.

Edmond, J. M.: High precision determination of titration alkalinity and total carbon dioxide content of sea water by potentiometric titration, Deep-Sea Res., 17, 737–750, https://doi.org/10.1016/0011-7471(70)90038-0, 1970.

Fay, A. R., Gregor, L., Landschützer, P., McKinley, G. A., Gruber, N., Gehlen, M., Iida, Y., Laruelle, G. G., Rödenbeck, C., Roobaert, A., and Zeng, J.: SeaFlux: harmonization of air–sea CO_2 fluxes from surface pCO_2 data products using a standardized approach, Earth Syst. Sci. Data, 13, 4693–4710, https://doi.org/10.5194/essd-13-4693-2021, 2021.

GMAO (Global Modeling and Assimilation Office): MERRA-2 tavgM_2d_flx_Nx: 2d, Monthly mean, Time-Averaged, Single-Level, Assimilation, Surface Flux Diagnostics V5.12.4, Greenbelt, MD, USA, Goddard Earth Sciences Data and Information Services Center (GES DISC) [data set], https://doi.org/10.5067/0JRLVL8YV2Y4, 2015.

Gregor, L. and Gruber, N.: OceanSODA-ETHZ: a global gridded data set of the surface ocean carbonate system for seasonal to decadal studies of ocean acidification, Earth Syst. Sci. Data, 13, 777–808, https://doi.org/10.5194/essd-13-777-2021, 2021.

Gruber, N., Clement, D., Carter, B. R., Feely, R. A., van Heuven, S., Hoppema, M., Ishii, M., Key, R. M., Kozyr, A., Lauvset, S. K., Lo Monaco, C., Mathis, J. T., Murata, A., Olsen, A., Perez, F. F., Sabine, C. L., Tanhua, T., and Wanninkhof, R.: The oceanic sink for anthropogenic CO_2 from 1994 to 2007, Science, 363, 1193–1199, https://doi.org/10.1126/science.aau5153, 2019a.

Gruber, N., Clement, D., Carter, B. R., Feely, R. A., Heuven, S., van, Hoppema, M., Ishii, M., Key, R. M., Kozyr, A., Lauvset, S. K., Lo Monaco, C., Mathis, J. T., Murata, A., Olsen, A., Perez, F. F., Sabine, C. L., Tanhua, T., and Wanninkhof, R.: The oceanic sink for anthropogenic CO_2 from 1994 to 2007 – the data (NCEI Accession 0186034), NOAA National Centers for Environmental Information [data set], https://doi.org/10.25921/wdn2-pt10, 2019b.

Hörstmann, C., Raes, E. J., Buttigieg, P. L., Lo Monaco, C., John, U., and Waite, A. M.: Hydrographic fronts shape productivity, nitrogen fixation, and microbial community composition in the southern Indian Ocean and the Southern Ocean, Biogeosciences, 18, 3733–3749, https://doi.org/10.5194/bg-18-3733-2021, 2021.

Huhn, F., A., von Kameke, V., Pérez-Muñuzuri, M. J., Olascoaga, and F. J., Beron-Vera: The impact of advective transport by the South Indian Ocean countercurrent on the Madagascar bloom, Geophys. Res. Lett., 39, L06602, https://doi.org/10.1029/2012GL051246, 2012.

Keppler, L., Landschützer, P., Gruber, N., Lauvset, S. K., and Stemmler, I.: Seasonal carbon dynamics in the near-

global ocean, Global Biogeochem. Cy., 34, e2020GB006571, https://doi.org/10.1029/2020GB006571, 2020.

Ko, Y. H., Lee, K., Takahashi, T., Karl, D. M., Kang, S.-H., and Lee, E.: Carbon-based estimate of nitrogen fixation-derived net community production in N−depleted ocean gyres, Global Biogeochem. Cy., 32, 1241–1252, https://doi.org/10.1029/2017GB005634, 2018.

Landolfi, A., Koeve, W., Dietze, H., Kähler, P., and Oschlies, A.: A new perspective on environmental controls of marine nitrogen fixation, Geophys. Res. Lett., 42, 4482–4489, https://doi.org/10.1002/2015GL063756, 2015.

Landschützer, P., Gruber, N., and Bakker, D.: Decadal variations and trends of the global ocean carbon sink, Global Biogeochem. Cy., 30, 1396–1417, https://doi.org/10.1002/2015GB005359, 2016.

Lauvset, S. K., Key, R. M., Olsen, A., van Heuven, S., Velo, A., Lin, X., Schirnick, C., Kozyr, A., Tanhua, T., Hoppema, M., Jutterström, S., Steinfeldt, R., Jeansson, E., Ishii, M., Perez, F. F., Suzuki, T., and Watelet, S.: A new global interior ocean mapped climatology: the $1^\circ \times 1^\circ$ GLODAP version 2, Earth Syst. Sci. Data, 8, 325–340, https://doi.org/10.5194/essd-8-325-2016, 2016.

Lauvset, S. K., Lange, N., Tanhua, T., Bittig, H. C., Olsen, A., Kozyr, A., Álvarez, M., Becker, S., Brown, P. J., Carter, B. R., Cotrim da Cunha, L., Feely, R. A., van Heuven, S., Hoppema, M., Ishii, M., Jeansson, E., Jutterström, S., Jones, S. D., Karlsen, M. K., Lo Monaco, C., Michaelis, P., Murata, A., Pérez, F. F., Pfeil, B., Schirnick, C., Steinfeldt, R., Suzuki, T., Tilbrook, B., Velo, A., Wanninkhof, R., Woosley, R. J., and Key, R. M.: An updated version of the global interior ocean biogeochemical data product, GLODAPv2.2021, Earth Syst. Sci. Data, 13, 5565–5589, https://doi.org/10.5194/essd-13-5565-2021, 2021a.

Lauvset, S. K., Lange, N., Tanhua, T., Bittig, H. C., Olsen, A., Kozyr, A., Álvarez, M., Becker, S., Brown, P. J., Carter, B. R., Cotrim da Cunha, L., Feely, R. A., van Heuven, S. M. A. C., Hoppema, M., Ishii, M., Jeansson, E., Jutterström, S., Jones, S. D., Karlsen, M. K., Lo Monaco, C., Michaelis, P., Murata, A., Pérez, F. F., Pfeil, B., Schirnick, C., Steinfeldt, R., Suzuki, T., Tilbrook, B., Velo, A., Wanninkhof, R., Woosley, R. J., and Key, R. M.: Global Ocean Data Analysis Project version 2.2021 (GLODAPv2.2021) (NCEI Accession 0237935), [subset used GLODAPv2.2021_Indian_Ocean.cvs], NOAA National Centers for Environmental Information [data set], https://doi.org/10.25921/ttgq-n825, 2021b.

Lee, K., Wanninkhof, R., Feely, R. A., Millero, F. J., and Peng, T. H.: Global relationships of total inorganic carbon with temperature and nitrate in surface seawater, Global Biogeochem. Cy., 14, 979–994, https://doi.org/10.1029/1998GB001087, 2000.

Lee, K., Karl, D. M., Wanninkhof, R., and Zhang, J. Z.: Global estimates of net carbon production in the nitrate-depleted tropical and subtropical oceans, Geophys. Res. Lett., 29, 1907, https://doi.org/10.1029/2001GL014198, 2002.

Lee, K., Tong, L. T., Millero, F. J., Sabine, C. L., Dickson, A. G., Goyet, C., Park, G. H., Wanninkhof, R., Feely, R. A., and Key, R. M.: Global relationships of total alkalinity with salinity and temperature in surface waters of the world's oceans, Geophys. Res. Lett., 33, L19605, https://doi.org/10.1029/2006GL027207, 2006.

Lévy, M., Shankar, D., André, J. M., Shenoi, S. S., Durand, F., and de Boyer Montegut, C.: Basin-wide seasonal evolution of the Indian Ocean's phytoplankton blooms, J. Geophys. Res., 112, C12014, https://doi.org/10.1029/2007JC004090, 2007.

Lewis, E. and Wallace, D. W. R.: Program developed for CO_2 system calculations, ORNL/CDIAC-105, Carbon Dioxide Information Analysis Center, Oak Ridge National Laboratory, US. Dept. of Energy, Oak Ridge, TN, 38 pp., 1998.

Lo Monaco, C. and Metzl, N.: Surface underway measurements of partial pressure of carbon dioxide (pCO_2), salinity, temperature and other associated parameters during the R/V Marion Dufresne OISO-30 cruise (EXPOCODE 35MV20200106) in Indian Ocean from 2020-01-06 to 2020-02-01 (NCEI Accession 0223954) [indicate subset used], NOAA National Centers for Environmental Information [data set], https://www.ncei.noaa.gov/archive/accession/0223954 (last access: 15 January 2021), 2021.

Lo Monaco, C., Metzl, N., Fin, J., Mignon, C., Cuet, P., Douville, E., Gehlen, M., Trang Chau, T. T., and Tribollet, A.: Distribution and long-term change of the sea surface carbonate system in the Mozambique Channel (1963–2019), Deep-Sea Res. Pt. II, 186–188, 104936, https://doi.org/10.1016/j.dsr2.2021.104936, 2021.

Longhurst, A.: A major seasonal phytoplankton bloom in the Madagascar Basin, Deep-Sea Res. Pt. I, 48, 2413–2422, https://doi.org/10.1016/S0967-0637(01)00024-3, 2001.

Louanchi, F., Metzl, N., and Poisson, A.: Modelling the monthly sea surface fCO_2 fields in the Indian Ocean, Mar. Chem., 55, 265–279, https://doi.org/10.1016/S0304-4203(96)00066-7, 1996.

Lueker, T. J., Dickson, A. G., and Keeling, C. D.: Ocean $pCO_{(2)}$ calculated from dissolved inorganic carbon, alkalinity, and equations for K-1 and K-2: validation based on laboratory measurements of CO_2 in gas and seawater at equilibrium, Mar. Chem., 70, 105–119, https://doi.org/10.1016/S0304-4203(00)00022-0, 2000.

Lutjeharms, J. R. E.: Remote sensing corroboration of retroflection of the East Madagascar Current, Deep-Sea Res., 35, 2045–2050, https://doi.org/10.1016/0198-0149(88)90124-0, 1988.

Menezes, V. V., Phillips, H. E., Schiller, A., Bindoff, N. L., Domingues, C. M., and Vianna, M. L.: South Indian countercurrent and associated fronts, J. Geophys. Res.-Oceans, 119, 6763–6791, https://doi.org/10.1002/2014JC010076, 2014.

Metzl, N.: Decadal increase of oceanic carbon dioxide in the Southern Indian Ocean surface waters (1991–2007), Deep-Sea Res. Pt. II, 56, 607–619, https://doi.org/10.1016/j.dsr2.2008.12.007, 2009.

Metzl, N., Poisson, A., Louanchi, F., Brunet, C., Schauer, B., and Bres, B.: Spatio-temporal distributions of air-sea fluxes of CO_2 in the Indian and Antarctic oceans, Tellus B, 47, 56–69, https://doi.org/10.3402/tellusb.v47i1-2.16006, 1995.

Metzl, N., Louanchi, F., and Poisson, A.: Seasonal and interannual variations of sea surface carbon dioxide in the subtropical indian ocean, Mar. Chem., 60, 131–146, https://doi.org/10.1016/S0304-4203(98)00083-8, 1998.

Metzl, N., Brunet, C., Jabaud-Jan, A., Poisson, A., and Schauer, B.: Summer and winter air-sea CO_2 fluxes in the Southern Ocean, Deep-Sea Res. Pt. I, 53, 1548–1563, https://doi.org/10.1016/j.dsr.2006.07.006, 2006.

Millero, F. J., Lee, K., and Roche, M.: Distribution of alkalinity in the surface waters of the major oceans, Mar. Chem., 60, 111–130, https://doi.org/10.1016/S0304-4203(97)00084-4, 1998.

Monteiro, F. M., Follows, M. J., and Dutkiewicz, S.: Distribution of diverse nitrogen fixers in the global ocean, Global Biogeochem. Cy., 24, GB3017, https://doi.org/10.1029/2009GB003731, 2010.

Montoya, J. P., Voss, M., Kahler, P., and Capone, D. G.: A simple, high-precision, high-sensitivity tracer assay for N_2 fixation, Appl. Environ. Microb., 62, 986–993, https://doi.org/10.1128/aem.62.3.986-993.1996, 1996.

Murata, A., Kumamoto, Y., Sasaki, K., Watanabe, S., and Fukasawa, M.: Decadal increases in anthropogenic CO_2 along 20° S in the South Indian Ocean, J. Geophys. Res., 115, C12055, https://doi.org/10.1029/2010JC006250, 2010.

Orr, J. C., Epitalon, J.-M., Dickson, A. G., and Gattuso, J.-P.: Routine uncertainty propagation for the marine carbon dioxide system, Mar. Chem., 207, 84–107, https://doi.org/10.1016/j.marchem.2018.10.006, 2018.

Palastanga, V., van Leeuwen, P. J., Schouten, M. W., and de Ruijter, W. P. M.: Flow structure and variability in the subtropical Indian Ocean: Instability of the South Indian Ocean Countercurrent, J. Geophys. Res., 112, C01001, https://doi.org/10.1029/2005JC003395, 2007.

Paulsen, H., Ilyina, T., Six, K. D., and Stemmler, I.: Incorporating a prognostic representation of marine nitrogen fixers into the global ocean biogeochemical model HAMOCC, J. Adv. Model. Earth Sy., 9, 438–464. https://doi.org/10.1002/2016MS000737, 2017.

Peng, T. H., Wanninkhof, R., Bullister, J. L., Feely, R. A., and Takahasi, T.: Quantification of decadal anthropogenic CO_2 uptake in the ocean based on dissolved inorganic carbon measurements, Nature, 396, 560–563, https://doi.org/10.1038/25103, 1998.

Pfeil, B., Olsen, A., Bakker, D. C. E., Hankin, S., Koyuk, H., Kozyr, A., Malczyk, J., Manke, A., Metzl, N., Sabine, C. L., Akl, J., Alin, S. R., Bates, N., Bellerby, R. G. J., Borges, A., Boutin, J., Brown, P. J., Cai, W.-J., Chavez, F. P., Chen, A., Cosca, C., Fassbender, A. J., Feely, R. A., González-Dávila, M., Goyet, C., Hales, B., Hardman-Mountford, N., Heinze, C., Hood, M., Hoppema, M., Hunt, C. W., Hydes, D., Ishii, M., Johannessen, T., Jones, S. D., Key, R. M., Körtzinger, A., Landschützer, P., Lauvset, S. K., Lefèvre, N., Lenton, A., Lourantou, A., Merlivat, L., Midorikawa, T., Mintrop, L., Miyazaki, C., Murata, A., Nakadate, A., Nakano, Y., Nakaoka, S., Nojiri, Y., Omar, A. M., Padin, X. A., Park, G.-H., Paterson, K., Perez, F. F., Pierrot, D., Poisson, A., Ríos, A. F., Santana-Casiano, J. M., Salisbury, J., Sarma, V. V. S. S., Schlitzer, R., Schneider, B., Schuster, U., Sieger, R., Skjelvan, I., Steinhoff, T., Suzuki, T., Takahashi, T., Tedesco, K., Telszewski, M., Thomas, H., Tilbrook, B., Tjiputra, J., Vandemark, D., Veness, T., Wanninkhof, R., Watson, A. J., Weiss, R., Wong, C. S., and Yoshikawa-Inoue, H.: A uniform, quality controlled Surface Ocean CO_2 Atlas (SOCAT), Earth Syst. Sci. Data, 5, 125–143, https://doi.org/10.5194/essd-5-125-2013, 2013.

Pierella Karlusich, J. J., Pelletier, E., Lombard, F., Carsique, M., Dvorak, E., Colin, S., Picheral, M., Cornejo-Castillo, F. M., Acinas, S. G., Pepperkok, R., Karsenti, E., de Vargas, C., Wincker, P., Bowler, C., and Foster, R. A.: Global distribution patterns of marine nitrogen-fixers by imaging and molecular methods, Nat. Commun., 12, 4160, https://doi.org/10.1038/s41467-021-24299-y, 2021.

Pierrot, D., Lewis, E., and Wallace, D. W. R.: MS Excel Program Developed for CO_2 System Calculations ORNL/CDIAC-105, Carbon Dioxide Inf. Anal. Cent., Oak Ridge Natl. Lab., U. S. Dept. of Energy, Oak Ridge, Tenn., https://cdiac.ess-dive.lbl.gov/ftp/co2sys/CO2SYS_calc_XLS_v2.1/ (last access: 3 March 2022), 2006.

Poisson, A., Metzl, N., Brunet, C., Schauer, B., Bres, B., Ruiz-Pino, D., and Louanchi, F.: Variability of sources and sinks of CO_2 in the western Indian and southern oceans during the year 1991, J. Geophys. Res., 98, 22759–22778, https://doi.org/10.1029/93JC02501, 1993.

Poulton, A. J., Stinchcombe, M. C., and Quartly, G. D.: High numbers of Trichodesmium and diazotrophic diatoms in the southwest Indian Ocean, Geophys. Res. Lett., 36, L15610, https://doi.org/10.1029/2009GL039719, 2009

Qi, L., Hu, C., Mikelsons, K., Wang, M., Lance, V., Sun, S., Barnes, B. B., Zhao, J., and Van der Zande, D.: In search of floating algae and other organisms in global oceans and lakes. Remote Sens. Environ., 239, 111659, https://doi.org/10.1016/j.rse.2020.111659, 2020.

Raj, R. P., Peter, B. N., and Pushpadas, D.: Oceanic and atmospheric influences on the variability of phytoplankton bloom in the Southwestern Indian Ocean, J. Marine Syst., 82, 217–229, https://doi.org/10.1016/j.jmarsys.2010.05.009, 2010.

Ramanantsoa, J. D., Penven, P., Raj, R. P., Renault, L., Ponsoni, L., Ostrowski, M., Dilmahamod, A. F., and Rouault, M.: Where and how the East Madagascar Current retroflection originates, J. Geophys. Res.-Oceans, 126, e2020JC016203, https://doi.org/10.1029/2020JC016203, 2021

Sabine, C. L., Wanninkhof, R., Key, R. M., Goyet, C., and Millero, F. J.: Seasonal CO_2 fluxes in the tropical and subtropical Indian Ocean, Mar. Chem., 72, 33–53, https://doi.org/10.1016/S0304-4203(00)00064-5, 2000.

Schlitzer, R.: Ocean Data View, http://odv.awi.de/ (last access: 17 May 2014), 2013.

Siedler, G., Rouault, M., and Lutjeharms, J. R. E.: Structure and origin of the subtropical South Indian Ocean Countercurrent, Geophys. Res. Lett., 33, L24609, https://doi.org/10.1029/2006GL027399, 2006.

Srokosz, M. A. and Quartly, G. D.: The Madagascar Bloom: A serendipitous study, J. Geophys. Res.-Oceans, 118, 14–25, https://doi.org/10.1029/2012JC008339, 2013.

Srokosz, M. A., Quartly, G. D., and Buck, J. J. H.: A possible plankton wave in the Indian Ocean, Geophys. Res. Lett., 31, L13301, https://doi.org/10.1029/2004GL019738, 2004.

Srokosz, M. A., Robinson, J., McGrain, H., Popova, E. E., and Yool, A.: Could the Madagascar bloom be fertilized by Madagascan iron?, J. Geophys. Res.-Oceans, 120, 5790–5803, https://doi.org/10.1002/2015JC011075, 2015.

Takahashi, T., Olafsson, J., Goddard, J. G., Chipman, D. W., and Sutherland, S. C.: Seasonal variation of CO_2 and nutrients in the high-latitude surface oceans: A comparative study, Global Biogeochem. Cy., 7, 843–878, https://doi.org/10.1029/93GB02263, 1993.

Takahashi, T., Sutherland, S. C., Sweeney, C., Poisson, A., Metzl, N., Tilbrook, B., Bates, N., Wanninkhof, R., Feely, R. A., Sabine, C., Olafsson, J., and Nojiri, Y.: Global Sea-Air CO_2 Flux Based on Climatological Surface Ocean pCO_2, and Seasonal Biological and Temperature Effect, Deep-Sea Res. Pt. II, 49, 9–10, 1601–1622, https://doi.org/10.1016/S0967-0645(02)00003-6, 2002.

Takahashi, T., Sutherland, S. C., Wanninkhof, R., Sweeney, C., Feely, R. A., Chipman, D. W., Hales, B., Friederich, G., Chavez, F., Sabine, C., Watson, A. J., Bakker, D. C., Schuster, U., Metzl, N., Yoshikawa-Inoue, H., Ishii, M., Midorikawa, T., Nojiri, Y., Körtzinger, A., Steinhoff, T., Hoppema, M., Olafsson, J., Arnarson, T. S., Tilbrook, B., Johannessen, T., Olsen, A., Bellerby, R., Wong, C., Delille, B., Bates, N., and de Baar, H. J.: Climatological mean and decadal change in surface ocean pCO_2, and net sea air CO_2 flux over the global oceans, Deep-Sea Res. Pt. II, 56, 554–577, https://doi.org/10.1016/j.dsr2.2008.12.009, 2009.

Takahashi, T., Sutherland, S. C., Chipman, D. W., Goddard, J. G., Ho, C., Newberger, T., Sweeney, C., and Munro, D. R.: Climatological distributions of pH, pCO_2, total CO_2, alkalinity, and $CaCO_3$ saturation in the global surface ocean, and temporal changes at selected locations, Mar. Chem., 164, 95–125, https://doi.org/10.1016/j.marchem.2014.06.004, 2014.

Tang, W. and Cassar, N.: Data-driven modeling of the distribution of diazotrophs in the global ocean, Geophys. Res. Lett., 46, 12258–12269, https://doi.org/10.1029/2019GL084376, 2019.

Tang, W., Li, Z., and Cassar, N.: Machine learning estimates of global marine nitrogen fixation, J. Geophys. Res.-Biogeo., 124, 717–730, https://doi.org/10.1029/2018JG004828 2019.

Touratier, F., Azouzi, L., and Goyet, C.: CFC-11, Δ14C and 3H tracers as a means to assess anthropogenic CO_2 concentrations in the ocean, Tellus B, 59, 318–325, https://doi.org/10.1111/j.1600-0889.2006.00247.x, 2007.

Uppström, L. R.: The boron/chlorinity ratio of deep-sea water from the Pacific Ocean, Deep-Sea Research and Oceanographic Abstracts, 21, 161–162, https://doi.org/10.1016/0011-7471(74)90074-6, 1974.

Uz, B. M.: What causes the sporadic phytoplankton bloom southeast of Madagascar?, J. Geophys. Res., 112, C09010, https://doi.org/10.1029/2006JC003685, 2007

Wanninkhof, R.: Relationship between wind speed and gas exchange over the ocean, J. Geophys. Res., 9, 7373–7382, https://doi.org/10.1029/92JC00188, 1992.

Wanninkhof, R.: Relationship between wind speed and gas exchange over the ocean revisited, Limnol. Oceanogr.-Methods, 12, 351–362, https://doi.org/10.4319/lom.2014.12.351, 2014.

Weiss, R. F.: Carbon dioxide in water and seawater: The solubility of a non-ideal gas, Mar. Chem., 2, 203–215, https://doi.org/10.1016/0304-4203(74)90015-2, 1974.

Weiss, R. F. and Price, B. A.: Nitrous oxide solubility in water and seawater, Mar. Chem., 8, 347–359, https://doi.org/10.1016/0304-4203(80)90024-9, 1980.

Westberry, T. K. and Siegel, D. A.: Spatial and temporal distribution of Trichodesmium blooms in the world's oceans, Global Biogeochem. Cy., 20, GB4016, https://doi.org/10.1029/2005GB002673, 2006.

Wilson, C. and Qiu, X.: Global distribution of summer chlorophyll blooms in the oligotrophic gyres, Prog. Oceanogr., 78, 107–134, https://doi.org/10.1016/j.pocean.2008.05.002, 2008.

Zeng, J., Matsunaga, T., Saigusa, N., Shirai, T., Nakaoka, S.-I., and Tan, Z.-H.: Technical note: Evaluation of three machine learning models for surface ocean CO_2 mapping, Ocean Sci., 13, 303–313, https://doi.org/10.5194/os-13-303-2017, 2017.